NSWCDD/TR-93/198

DESIGN VALIDATION TESTS ON A REALISTIC HYPERSONIC WAVERIDER AT MACH 10, 14, AND 16.5 IN THE NAVAL SURFACE WARFARE CENTER HYPERVELOCITY WIND TUNNEL NO. 9

BY MARK E. KAMMEYER AND MICHAEL J. GILLUM

STRATEGIC AND SPACE SYSTEMS DEPARTMENT

5 MAY 1994

NAVAL SURFACE WARFARE CENTER
DAHLGREN DIVISION • WHITE OAK DETACHMENT
Silver Spring, Maryland 20903-5640

NSWCDD/TR-93/198

DESIGN VALIDATION TESTS ON A REALISTIC HYPERSONIC WAVERIDER AT MACH 10, 14, AND 16.5 IN THE NAVAL SURFACE WARFARE CENTER HYPERVELOCITY WIND TUNNEL NO. 9

BY MARK E. KAMMEYER AND MICHAEL J. GILLUM
STRATEGIC AND SPACE SYSTEMS DEPARTMENT

5 MAY 1994

NAVAL SURFACE WARFARE CENTER
DAHLGREN DIVISION • WHITE OAK DETACHMENT
Silver Spring, Maryland 20903-5640

FOREWORD

This report covers wind tunnel testing of a realistic hypersonic waverider vehicle. The work was sponsored by the McDonnell Douglas Space Systems Company, Huntington Beach, and the United States Air Force Ballistic Missile Organization, Norton Air Force Base.

Tests were conducted in the Navy's Hypervelocity Wind Tunnel No. 9 located at the White Oak, Maryland site of the Dahlgren Division, Naval Surface Warfare Center. Model fabrication was performed by the Division's Engineering Prototype Branch.

The waverider was tested at Mach numbers of 10, 14, and 16.5 to measure static stability and drag, to determine the distributions of surface pressure and heat transfer, and to obtain flow-visualization data. The two principal objectives of this test program were to validate the methodology for designing performance-optimized hypersonic waveriders and to obtain data on a complex hypersonic configuration for validation of computational fluid dynamics codes.

Approved by:

R. L. SCHMIDT, Head
Strategic and Space Systems Department

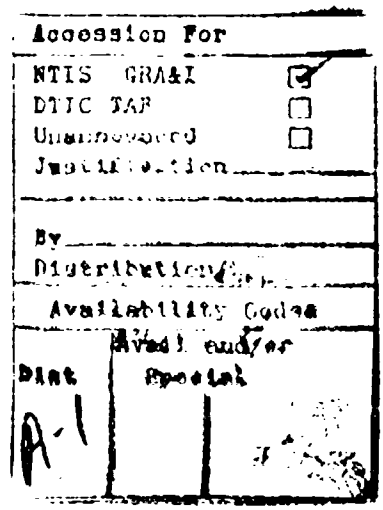

ABSTRACT

A realistic hypersonic waverider was tested in the Navy's Hypervelocity Wind Tunnel No. 9 in late Spring of 1993. Sponsored by the McDonnell Douglas Space Systems Company, Huntington Beach, and the United States Air Force Ballistic Missile Organization, Norton Air Force Base, tests at Mach numbers of 10, 14, and 16.5 were conducted to measure static stability and drag, to determine the distributions of surface pressure and heat transfer, and to obtain flow-visualization data.

The two principal objectives of this test program were to validate the methodology for designing performance-optimized hypersonic waveriders and to obtain data on a complex hypersonic configuration for validation of computational fluid dynamics codes. The waverider design included realistically blunted leading edges and was optimized on an arbitrary figure of merit to include fluid viscosity and internal volume. The design condition of Mach 14 and Reynolds number based on length of 6.5 million was chosen based on the facility capabilities.

All data appeared to be independent of Mach number and virtually insensitive to changes in Reynolds number; moreover, all data displayed excellent repeatability. The lift-to-drag ratio of this waverider with realistic leading-edge radii was found to be relatively high.

CONTENTS

ILLUSTRATIONS

ILLUSTRATIONS (CONTINUED)

TABLES

INTRODUCTION

This document is the final report for the McDonnell Douglas/United States Air Force Ballistic Missile Organization Waverider Design Validation Test. The test was conducted in the Navy's Hypervelocity Wind Tunnel No. 9 between 17 May and 9 June 1993. Tunnel 9 is located at the White Oak, Maryland site of the Dahlgren Division, Naval Surface Warfare Center (NSWC). The test objectives were twofold. The first objective was to validate a methodology for designing performance-optimized hypersonic waveriders which incorporate realistic leading-edge radii. Fluid viscosity and vehicle internal volume were included in the optimization. The second objective was to measure surface pressure and heat transfer on a complex hypersonic configuration for validation of computational fluid dynamics codes. Static stability and drag, distributions of surface pressure and heat transfer, and flow-visualization data were obtained at nominal Mach numbers of 10, 14, and 16.5.

The sponsors of this test program were the McDonnell Douglas Space Systems Company, Huntington Beach, California, and the USAF Ballistic Missile Organization (BMO), Norton AFB, California. The McDonnell Douglas project manager was Mr. David Burnett. The BMO project managers were CAPT. Patrick Obrien and LT. Doug Fullingim. Additional test support was provided by Ms. Tobenette Holtz of TRW Corp. The Tunnel 9 project engineer was Mr. Mark E. Kammeyer, assisted by Mr. Michael J. Gillum. All questions concerning this test report should be directed to Mr. Kammeyer, Code K24.

TEST FACILITY

The NSWC Hypervelocity Wind Tunnel No. 9 is a blow-down facility which operates at Mach numbers of 8, 10, 14, and most recently, 16.5. Maximum Reynolds numbers are approximately 50×10^6 per foot at Mach 8, 20×10^6 per foot at Mach 10, 3.8×10^6 per foot at Mach 14, and 3.2×10^6 per foot at Mach 16.5. The test cell is 5 feet in diameter and is over 12 feet long. This allows the testing of large model configurations. A photograph of Tunnel 9 is shown in Figure 1.

Tunnel 9, shown schematically in Figure 2, uses nitrogen as the working fluid. During a typical run, the vertical heater vessel is used to pressurize and heat a volume of nitrogen to a predetermined pressure and temperature. The test section and vacuum sphere are evacuated to a low pressure and are separated from the heater by a pair of metal diaphragms. When the nitrogen in the heater reaches the proper temperature and pressure, the diaphragms are ruptured and the gas flows from the top of the heater and expands through the nozzle. As the hot gas exits the heater, cold gas from three pressurized driver vessels enters the heater base. The cold gas drives the hot gas in a piston-like fashion, thereby maintaining constant conditions in the test cell during the run. More detailed information concerning the facility can be obtained from Reference 1. Nominal tunnel conditions for this test program are listed in Table 1.

MODEL HARDWARE

The aerodynamic design of the wind-tunnel model was carried out by McDonnell Douglas, with fabrication performed by NSWC personnel. An electronic design was maintained from the aerodynamic definition through fabrication. A few details are presented in order to familiarize the reader with the methodology.

AERODYNAMIC DESIGN

The process used to generate the waverider shape is described in detail in Reference 2. A modified version of the University of Maryland Axisymmetric Waverider Program (MAXWARP) code was used to generate a sharp-edged waverider optimized on a figure of merit which encompassed viscous L/D, volume, and wetted area. The design condition of Mach 14, Re_L = 6.5 million, was chosen based upon the facility capabilities. The resulting geometry was in the form of body coordinates at a specified number of cross sections. Using a CAD system, splines were fit through the points to create a wire-frame model. The model was split at the sharp edge. The upper and lower halves were separated far enough to accommodate a leading edge with a radius of 0.25 inch. The final design had an overall length of 39 inches, a span of 16.161 inches, and a base height of 6.839 inches. The planform and base areas were 375.3 and 64.6 square inches, respectively. The planform area was selected as the reference area for defining aerodynamic coefficients.

MODEL FABRICATION

The wire-frame geometry, shown in Figure 3, was transferred electronically from McDonnell Douglas to NSWC for fabrication of a wind tunnel model. The data were read into a solid-modeling CAD system. Surfaces were fit to the wire-frame model and a solid model created. The solid model was then broken into sections for the mechanical design. Upon completion of the mechanical design, tool paths were generated for the parts and post-processed for computer numerically controlled (CNC) machining. An aluminum prototype model was fabricated to ensure that the desired geometry was properly reproduced. The details of this process are presented in Reference 3.

The test article was fabricated in eight parts. The body consisted of four sections manufactured from 6061-T6 aluminum. The nose, both leading edges, and the main cavity cover plate were manufactured from 17-4 PH stainless steel. The final step was hand finishing of the surfaces to remove tool marks. A photograph of the model mounted in the tunnel is shown in Figure 4.

INSTRUMENTATION

TUNNEL INSTRUMENTATION

The instrumentation used to monitor the wind tunnel conditions included one transducer to measure supply pressure, two thermocouples to measure supply temperature, and two Pitot tubes in the tunnel test cell. The two thermocouples and the two Pitot tubes are used for reliability, and readings are averaged when both are felt to be reliable. The supply-temperature thermocouples were fabricated at NSWC. The angular position of the model support system was measured with a reel-type readout potentiometer attached to the tunnel sector mechanism. The specific types of tunnel instrumentation used are outlined in Table 2.

MODEL INSTRUMENTATION

The model was instrumented with a six-component balance to measure forces and moments, 32 pressure transducers, and 48 coaxial thermocouples. The measurement of static stability and drag were considered primary. All instrumentation

was provided and installed by Tunnel 9 personnel. The specific types of model instrumentation used are outlined in Table 3.

Force Balance

The force balance used for this test program was an Able Corporation 1.5 inch Mk 34a with the Tunnel 9 designation of 9HV6-3. The maximum load ratings for this balance were as follows:

Normal force:	2000 lbf
Yaw force:	500 lbf
Axial force:	600 lbf
Roll moment:	800 in-lbf

Pressure Instrumentation

Pressures were measured at 32 locations on the model: 24 on the body and eight on the base. The body pressures were arranged along rays emanating from the model nose and confined to the left half of the model. This is illustrated in Figures 5(A-C). The naming nomenclature and coordinate locations of the taps are given in Table 4. The locations of the base pressure taps are shown in Figure 5(D). With two exceptions, all pressure taps on the model used stainless steel tubing with an inside diameter of 0.062 inch. The gages were Kulite model XCW-062-5A transducers, and were connected to the taps with short lengths of flexible Tygon tubing. These gages have a nominal rating of 5 psia. Tubing lengths were limited to one inch or less in order to minimize lag, as outlined in Reference 1.

The exceptions were at locations P3G and P9G. These gages were Kulite model XCW-093-15A transducers, nominally rated at 15 psia. They incorporated special screens consisting of a single pinhole, 0.031 inch in diameter, and were mounted flush with the external surface. This was done in order to study the spectral content of the pressure signal. The results of this effort will be reported under separate cover.

Heat-Transfer Instrumentation

Measurements of surface temperature rise and heat transfer were made using Medtherm model TCS-E-10370 coaxial thermocouples. The thermocouple materials

were chromel and constantan. The gages were cemented into the model using Loctite No. 271 adhesive and sanded to conform to the external contours; the sanding formed the thermal junction. Locations and nomenclature are presented in Figures 5(A-C) and Table 4. Complete information regarding the coaxial thermocouple technique can be found in References 4 and 5.

Temperature-sensitive Paint

Runs 2393 and 2395 explored the feasibility of a temperature-mapping flow-visualization technique. The technique, as researched at Purdue University, exploits the temperature-dependent fluorescent quantum efficiency of the rare-earth chelate europium thenoyltrifluoroacetonate. The fluorescent intensity can be measured with a photo-diode, and a correlation between photo-diode output and temperature can be determined. The objectives of the effort were to obtain detailed visualization of boundary-layer transition and leading-edge vortices, as well as quantitative mapping of the surface heat transfer. More detailed information concerning this technique, and its results as applied to this test program, can be obtained from Reference 6.

TEST CONDUCT

RUN PROCEDURE

Preparations for a tunnel run began with setting the model orientation in the tunnel and securing the test cell and tunnel room. The heater vessel was then charged to its initial pressure, and pressurization of the driver vessels was begun. Calibrations of the pressure instrumentation were then performed. First, the tunnel supply-pressure transducer was calibrated in place. A series of shunt resistances simulating known pressures were applied to the transducer, and the output recorded, allowing a calibration curve to be computed. Calibration of the test-cell Pitot and model pressure transducers was then performed by recording data while the test cell was evacuated from atmospheric pressure to approximately 1 mmHg. Two MKS Baratron type 145 transducers with ranges of 1000 and 10 mmHg monitored the test-cell pressure and were used as the reference standards. The evacuation was halted briefly when calibration data were recorded to ensure uniform pressure in the test cell.

After the tunnel evacuation was completed, static tare readings were recorded with the model at a fixed angle of attack. Next, dynamic tare readings were recorded during a wind-off pitch sweep. The 25-minute heating cycle was then begun. Another static tare was recorded toward the end of the heating, approximately two minutes before the run. When the desired supply conditions were reached, the tunnel run was initiated by bursting the two metal diaphragms. After flow was established, the model was pitched through a wind-on sweep identical to that used for the dynamic tare.

For the majority of the runs, the model support system was programmed to hold the model at zero angle of attack until the starting shock wave had passed. Then the model was pitched to -10° while the starting transients died out. The sweep from -10° to +25° was timed to occur during the equilibrium portion of the run. After the hot gas was exhausted, the model was brought back to zero. For run 2394, the shorter run time dictated that the model be held at -10° during tunnel start-up and that the sweep begin from that position. The maximum angle of attack for this run was also limited to +4° by the balance capacity.

Wind-off loads were computed from the static and dynamic tare data taken before heating. The wind-on loads were computed from the pre-run static tare and the wind-on data. Aerodynamic loads were determined by subtracting the wind-off loads from the wind-on loads at the same pitch angle. The pre-run static tare data were also used to update the pressure transducer calibrations, using a reading from the 0-10 mmHg reference transducer. This procedure corrects for any transducer drift during heating and improves the accuracy of the calibrations at low pressures.

DATA ACQUISITION

Data were sampled and recorded using the Tunnel 9 Data Acquisition and Recording Equipment (DARE) VI. DARE VI is a simultaneous-sample-and-hold, single-amplifier-per-channel system with 14-bit resolution. The output signals of all the instrumentation were amplified and fed through six-pole low-pass Bessel filters with a cutoff frequency of 25 Hz before being recorded. The analog filters removed most 60-Hz electrical noise. The sample rate was 250 Hz for all of the runs.

DATA REDUCTION

All acquired data were reduced unless believed to be in error or extraneous. A list of all inoperative transducers for each run is presented in Table 5.

Digital Filtering

In addition to the analog filters used on all channels, the data were filtered during data reduction using a low-pass, sixth-order Butterworth digital filter. A cutoff frequency of 10 Hz was used for filtering the tunnel supply temperature and pressure data, the tect cell Pitot data, and all of the model temperature and pressure gage data. Force-balance data were filtered based on the vibration frequencies of the particular combination of sting, balance, and model. A cutoff frequency of 5 Hz was used for the normal-force, pitching-moment, and axial-force data. The side-force, yawing-moment, and rolling-moment data were filtered using a cutoff frequency of 3 Hz. The data were filtered both forward and backward to prevent the introduction of time lag.

Tunnel Conditions

The supply and Pitot pressures were determined from their respective calibrations, as outlined above. The supply temperature was determined from the NIST tables for the thermocouple materials. The tunnel conditions were calculated from these quantities using real gas thermodynamics, as outlined in Reference 1.

Force Data

Balance loads were computed using a calibration performed prior to the test entry. The calibration included first-order interaction effects.[7] A balance and sting bending calibration was used to correct the measured pitch and yaw angles for bending of the sting due to the model weight and aerodynamic load. The force data were reduced to coefficient form in both the body-axes and the stability-axes coordinate systems. The definitions of axes systems, aerodynamic angles, and all transformation equations used in the data reduction program are consistent with those given in References 7 and 8.

Pitching and yawing moments measured about the balance center were transferred to the model moment reference center (MRC) using reference measurements made during installation. A base drag correction was applied to the measured axial force to obtain corrected axial-force coefficients in the body axes. The base pressure coefficient was computed as an integration of the eight base pressure measurements. The areas assigned to each base pressure tap are presented in Table 6. No base drag corrections were done in the stability axes. The reference lengths and areas used are summarized in the data tabulations, and can also be found in the nomenclature.

Pressure Data

The pressure data were reduced in units of psia as well as the nondimensional forms P/PINF and CP.

Heat-Transfer Data

The millivolt output of each coaxial thermocouple was converted to surface temperature rise using the conversion factor for chromel-constantan thermocouples. A heating rate was computed from each temperature rise using a finite-difference solution of the unsteady, one-dimensional, heat-conduction equation for a homogeneous planar slab of finite thickness, as discussed in References 4 and 5. The thermocouples were mounted in 17-4 PH stainless steel, using plugs in those parts which were aluminum. The lumped thermal properties of 17-4 steel, chromel, and constantan are essentially equivalent, justifying the assumption of material homogeneity. A uniform initial temperature was assumed, and the inside surface of the model was assumed to experience zero heat transfer. The measured temperature rise at the heated surface provided the remaining boundary condition needed to compute the temperature distribution within the slab. Temperatures were calculated at 50 node points in the slab, and the heating rate was computed from the temperature gradient at the surface and the thermal conductivity of the gage material. Calculations were also performed with 20 and 100 nodes; these calculations showed that the solutions were converged with 50 nodes.

The assumption of one-dimensional planar heat conduction was not valid for gages TN, T2D2, T2D3, T5D3, T5D4, and T5D5. For these gages, a cylindrical implementation of the one-dimensional heat equation was used. While the cylindrical equation was more realistic, the heating was two or three dimensional. This should be kept in mind when interpreting the data.

Photographic Data

Photographic data for this test program consisted of 35-mm color setup shots, and 16-mm and 70-mm color schlieren flow-visualization photographs. The 16-mm camera was operated at a rate of 500 frames per second. The 70-mm camera was operated at approximately 20 frames per second. Timing marks were recorded on each frame, along with the date and the run number. Example photographs from the 70-mm camera during runs 2388 and 2391 are presented in Figures 6 and 7, respectively.

MEASUREMENT UNCERTAINTY

Measurement uncertainties were estimated using the principles set forth in Reference 9, using specific procedures for Tunnel 9 given in Reference 10. In general, the uncertainty in a measurement was composed of a combination of fixed error or bias, B, and random error or precision, P. The root-sum-square model was used to estimate the uncertainties at the 95% confidence level:

$$U_{rss} = \pm\left[B^2 + P^2\right]^{1/2}$$
$$= \pm\left[B^2 + (t_{95}S)^2\right]^{1/2}$$

where U_{rss} is the uncertainty, S is the sample standard deviation, and t_{95} is the 95th percentile point for the two-tailed Student's "t" distribution (95-percent confidence interval). For sample sizes greater than 30, t_{95} is considered equal to 2. Bias and precision errors were propagated through to calculated parameters individually, then combined into overall uncertainties using the method given in Reference 11. Estimated uncertainties are presented in Tables 2, 3, 7, and 8. Traceability of working standards to the National Institute of Standards and Technology is maintained through the Navy Metrology and Calibration (METCAL) Program[12] and through manufacturer-provided calibrations.

DISCUSSION

A total of eight tunnel runs were accomplished in this test program. The test matrix is summarized in Table 9. Runs were first performed at the waverider's design point of Mach 14 and a unit Reynolds number of 2.0 x 10^6/ft. Two pitch-sweep runs (2387, 2389) and one yaw-sweep run (2388) were performed at these conditions. The pitch-sweep run was repeated because the first fifteen degrees of sweep for run 2387 occurred while condensed flow still existed in the test cell. The run was successfully repeated (run 2389) to include the full pitch sweep of interest. Runs were also performed to investigate the effects of off-design Mach numbers (runs 2390 and 2391) and the effects of Reynolds number (run 2394). Runs 2393 and 2395 were performed to investigate the temperature-sensitive paint,[6] but these runs also provided data to assess repeatability.

Two sets of runs could be used to assess facility repeatability and flow angularity/model misalignment. Runs 2387 and 2389 provided repeat data for angles

of attack between 5 and 25 degrees at Mach 14, Re = 2.0 x 10^6/ft. Runs 2391, 2393, and 2395 provide repeat data for angles of attack between -10 and 10 degrees at Mach 10, Re = 2.0 x 10^6/ft. Run 2393 was performed with the model at a fixed angle of attack, allowing comparisons of fixed versus sweep data. Run 2395 was performed with the model/balance/sting rolled 180 degrees, allowing an assessment of flow angularity/model misalignments.

The data appeared to be consistent and repeatable. However, two points need to be made. First, it was discovered during testing that the sting support was not aligned with the tunnel centerline. Position measurements showed that the model was mounted squarely on a sting that was yawed 0.9 degrees to the right. This resulted in a non-zero BETA on the pitch-sweep runs and an increased ALPHA on the yaw-sweep run. The effects could be seen in the data, e.g. a rolling-moment trend. Second, on run 2388, YFC and YMC were not zero at BETA = 0 degrees. Constant increments of 0.00241 and 0.00158 were respectively added to YFC and YMC for run 2388 to shift the curves through zero at BETA = zero. The error is attributed to bias in the balance yaw-force and yaw-moment measurements. No other data corrections were performed.

Analyses were performed on the force and moment data, the pressure data, and the heat-transfer data. Each of these types of data will be discussed here separately, focusing on both the qualitative and quantitative aspects of the data as well as the overall repeatability observed for all the runs.

FORCE/MOMENT DATA

Design Mach Number

Perhaps the most distinguishing piece of information about the performance of any waverider is its lift-to-drag ratio (L/D). The L/D of this waverider with realistically blunted leading edges was found to be relatively high. Figure 8 shows the L/D for the design condition of Mach 14, Reynolds Number of 2.0 x 10^6/ft. Runs 2387, 2388, and 2389 are all plotted here and appear to be in excellent agreement. This is the first of many plots that show the tunnel's excellent repeatability. Figures 9 to 11 are plots of CLS, CDS, PMCS, and XCPP vs. angle of attack, ALPHA, for runs at the design Mach number.

Yaw Sweep

Run 2388 was a yaw sweep. The model had a constant angle of attack of about 1.09 degrees throughout the full sweep. Figures 12 to 15 are plots of L/D, CLS, CDS, YMCS, and XCPY vs. angle of side slip, BETA.

Mach-Number Effects

To further emphasize repeatability while introducing the Mach-number independence observed during the test program, Figures 16 to 19 show L/D, CLS, CDS, PMCS, and XCPP vs. ALPHA for three different Mach numbers: Mach = 14 (run 2389), Mach = 16.5 (run 2390), and Mach = 10 (run 2391). These coefficients appear to be virtually insensitive to the changes in Mach number.

Reynolds-Number Effects

Figures 20 to 23 show L/D, CLS, CDS, PMCS, and XCPP vs ALPHA for all of the Mach-10 runs. All runs except run 2394 were for a Reynolds number of 2.0 x 10^6/ft. Run 2394 had a Reynolds number for 20 x 10^6/ft. Notice that there is only a slight difference in the character of these curves. Furthermore, for run 2395 the model was rolled 180 degrees and tested upside down. This enabled data to be taken to the more negative angles of attack, while again showing tunnel repeatability.

Drag Polar

Another excellent example of tunnel repeatability, Mach-number independence, and Reynolds-number effects was a plot of the drag polar for all runs. Figure 24 is a plot of CLS vs. CDS for all eight runs. Again, excellent agreement was found.

PRESSURE DATA

Since the model was instrumented with gages on the top surface, bottom surface, base, and leading edges, a map of pressures for virtually the entire body could be assembled. These pressure data were somewhat useful in trying to quantify the location and strength of the shock wave as it spilled over the leading edges.

Design Mach Number

Figure 25 is a plot of pressure coefficient, CP, vs. ALPHA for a gage located on the top centerline and for one on the bottom centerline. Gages P2A and P2G from runs 2387 and 2389 were chosen here.

Mach-Number Effects

Figure 26 is a plot of CP vs. ALPHA for gages P2A and P2G for three different Mach numbers. Runs 2389, 2390 and 2391 were chosen here. Figures 27 to 29 are plots of the axial surface pressure coefficient variations along the top and bottom centerline rays of the model at -10°, 0° and 10° angle of attack. Surface pressures on the leeward surface were significantly lower than those measured on the windward surface. This seemed to be a result of the shock containment around the leading edge. The same trend was seen with the heat-transfer data, as would be expected.

With only two pressure gages around the leading edge, it was difficult to say much about the location of the shock, other than to bound its strength. Figure 30 shows the changes in the two leading-edge gages, P6D1 and P6D2, with angle of attack for runs at Mach numbers 14, 16 5, and 10. The windward gage sees a much stronger portion of the leading-edge shock than the leeward gage, which measures a lower value. Although this may be intuitively obvious, this trend helps to qualitatively check the gage output.

Base pressures were expected to be only a fraction of free-stream pressure. Figure 31 shows the variation in the average base pressure with angle of attack for Mach numbers 14, 16.5, and 10. The respective variations in free-stream pressure, PINF, are also shown for each Mach number.

HEAT-TRANSFER DATA

Design Mach Number

Figure 32 is a plot of Stanton Number, ST, vs. ALPHA for a gage located on the top centerline and one on the bottom centerline. Gages T3A and T3G from runs 2388 and 2389 were chosen here.

Mach-Number Effects

Figure 33 is a plot of ST vs. ALPHA for gages T3A and T3G for three different Mach numbers. Runs 2389, 2390 and 2391 were chosen here. Figures 34 to 36 are plots of top and bottom centerline axial Stanton number distributions for angles of attack equal to -10°, 0° and 10°, respectively. Large, abrupt changes in heat transfer along the surface of the model may be attributed to transition from laminar to turbulent flow. The approximate location of transition may be seen to move forward as pitch angle is increased.

The cluster of five thermocouples and the reduced heat-transfer data provided a slightly better understanding of how the strength of the leading-edge shock varies from the bottom to the top surface. Figure 37 shows the heating rates detected at these gage locations as a function of angle of attack. As with the pressure gage's data trend, a change from higher heating to a lower heating as one moves from the windward gage to the leeward gage is obvious.

Theoretically, an infinitely sharp leading edge would have an attached shock everywhere along it, thus preventing any spill-over of fluid from the bottom surface, where pressures are high, to the top surface, where pressures are very low. Even for a blunted leading edge, there seemed to be some shock containment, and spill-over was not occurring to a significant degree. This was a result of the detached shock's becoming much weaker as it wrapped around the leading edge. The measurements of both pressure and heat transfer support this shock-containment theory.

TEST DATA PACKAGE

The final data package to McDonnell Douglas and the Air Force consisted of the photographic data and magnetic computer tapes; the tapes contained full listings and thinned tabulations of:

- Wind tunnel conditions
- Static stability and drag data in body-axes coordinates
- Static stability and drag data in stability-axes coordinates
- Surface pressure data in
    1) Absolute pressure in psia
    2) Pressure ratio P/PINF

3) Pressure coefficient CP

Aerodynamic heating data in

1) Surface temperature rise in degrees R
2) Heating rate BTU/ft^2-sec
3) Stanton number

FORTRAN routines were included for reading and plotting the data. In addition, the data were interpolated for integer values of the angle of attack. Requests for data should be directed to:

Naval Surface Warfare Center Dahlgren Division
White Oak Detachment, Code K24, Bldg. 402
10901 New Hampshire Avenue
Silver Spring, Maryland 20903-5640

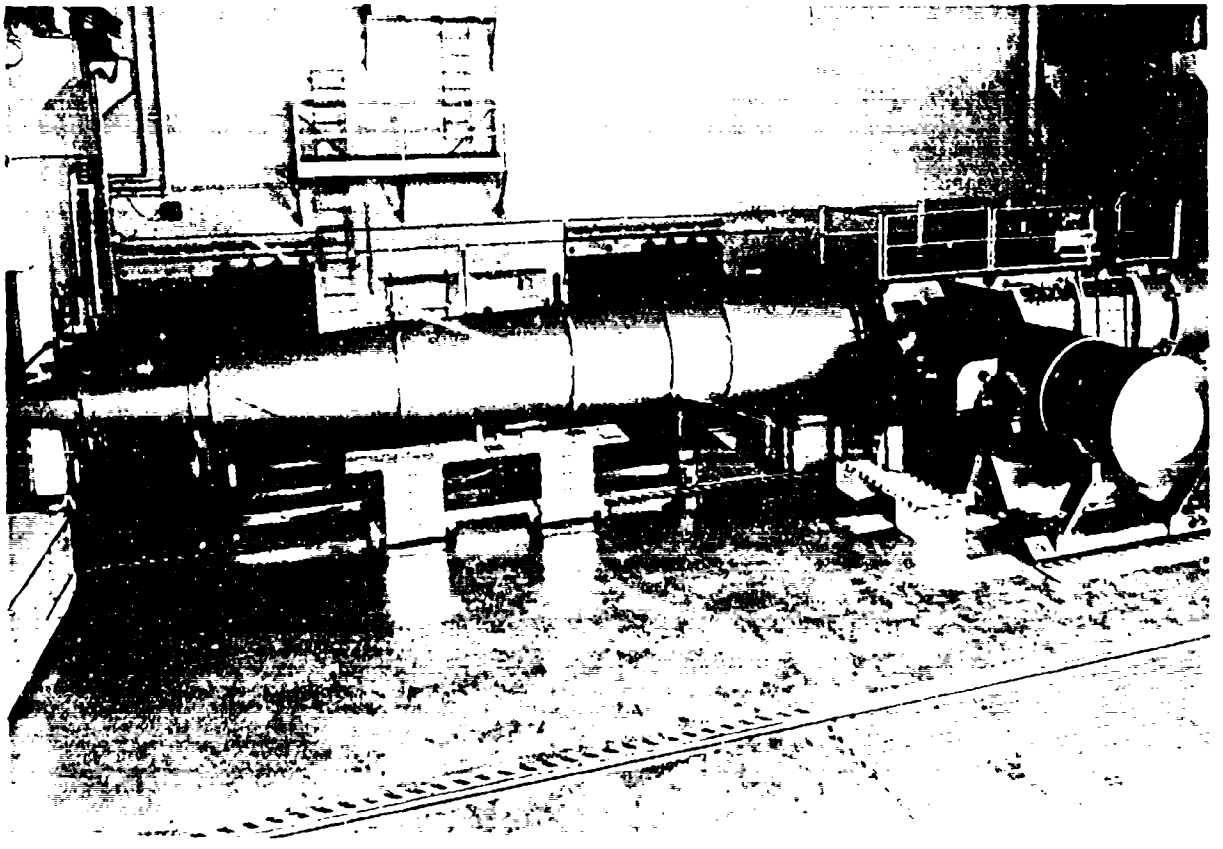

FIGURE 1. NSWC HYPERVELOCITY TUNNEL 9

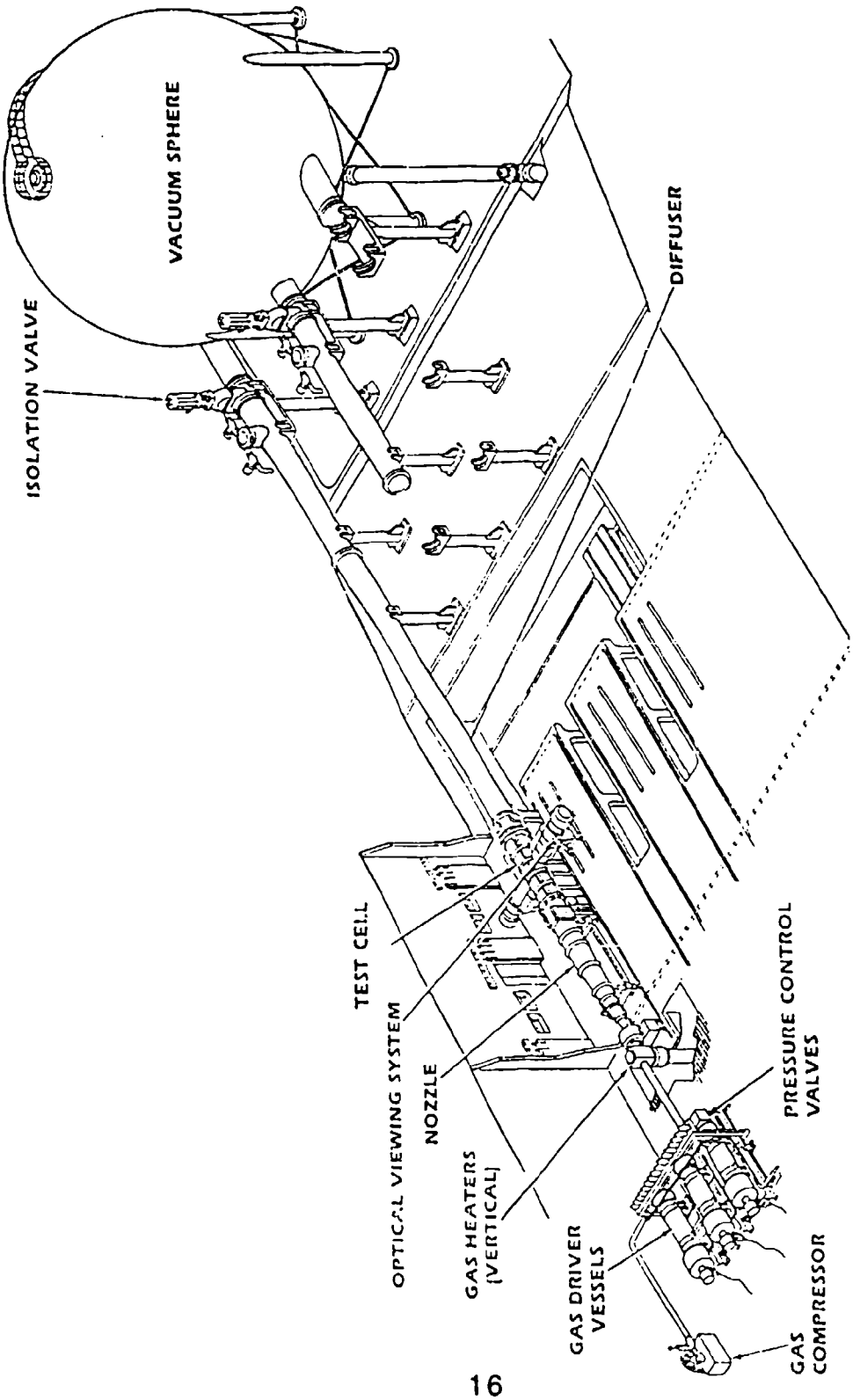

FIGURE 2. SCHEMATIC OF NSWC HYPERVELOCITY TUNNEL 9

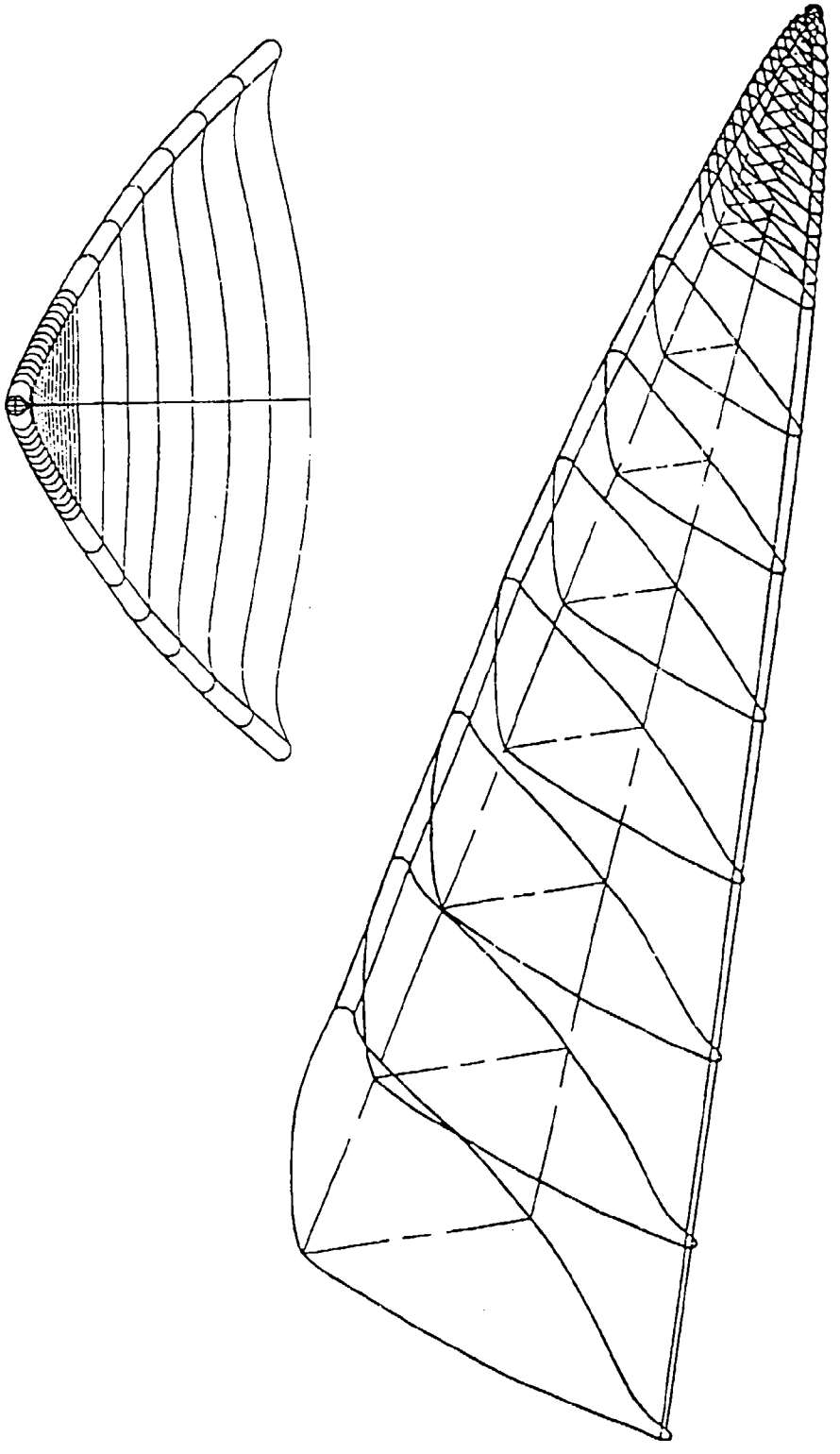

FIGURE 3. CAD DRAWING OF WAVERIDER WIRE-FRAME DESIGN

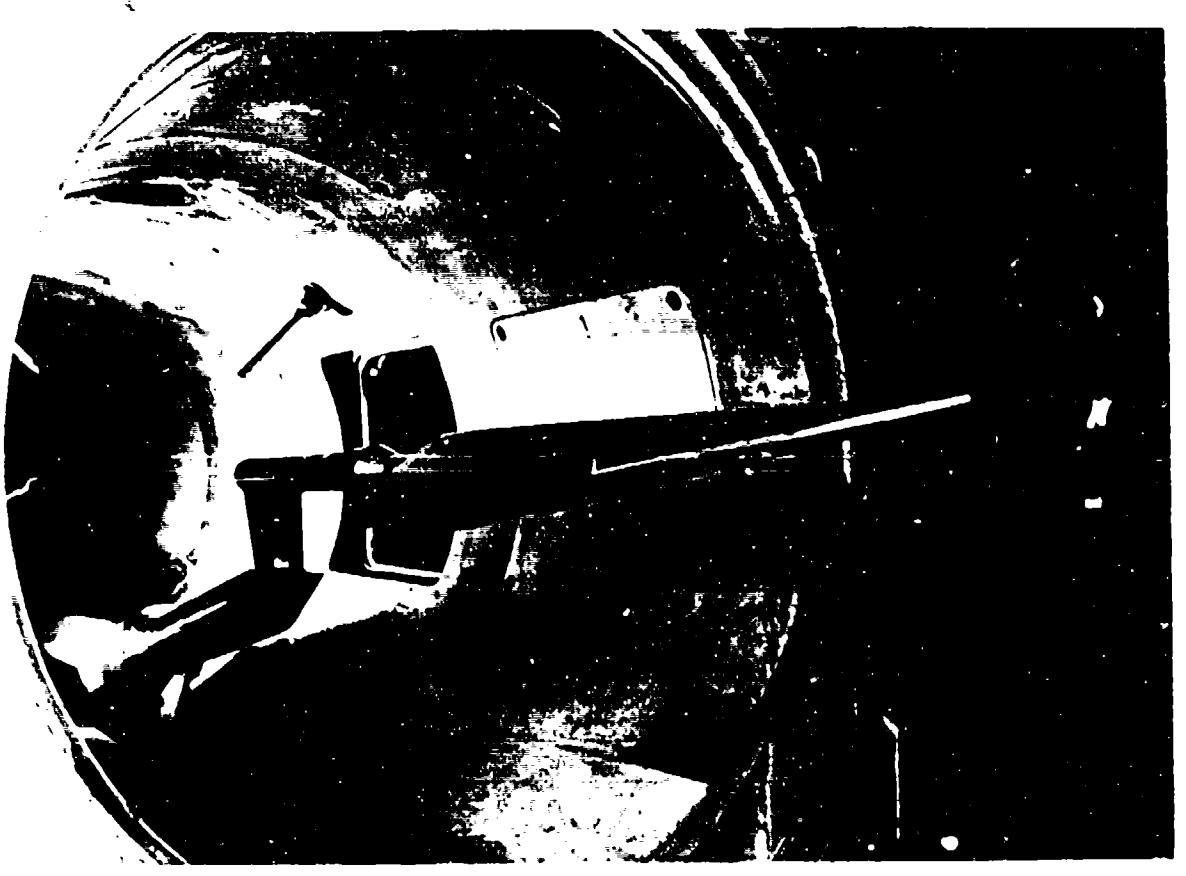

FIGURE 4. WAVERIDER MODEL MOUNTED IN TUNNEL 9

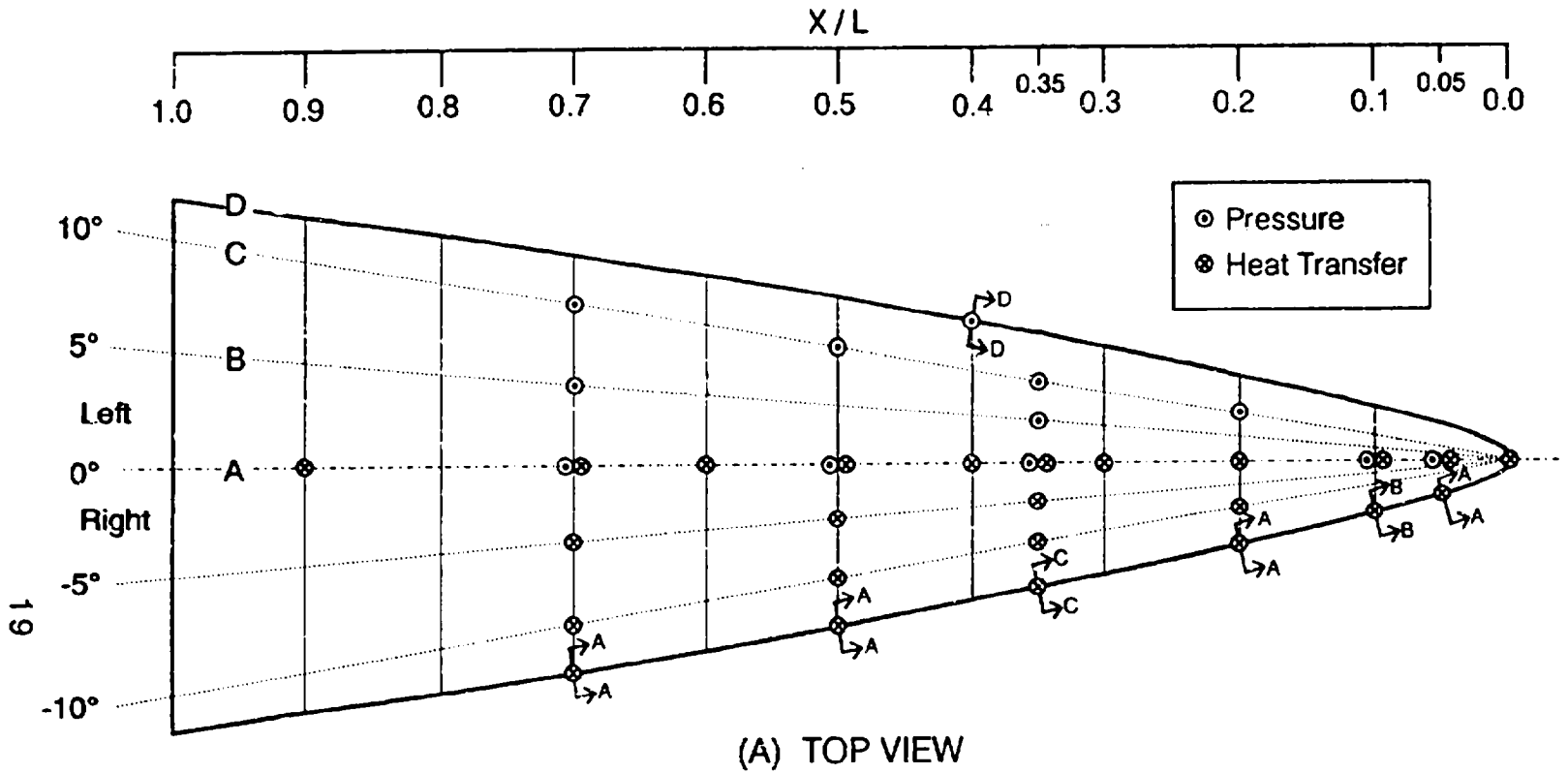

(A) TOP VIEW

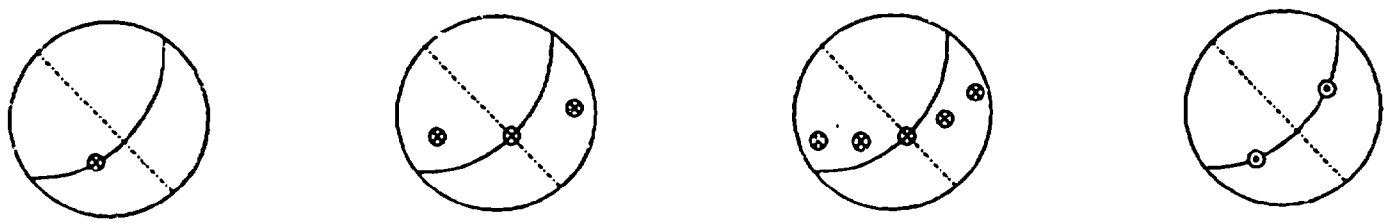

(B) LEADING-EDGE VIEW

FIGURE 5. INSTRUMENTATION LOCATIONS

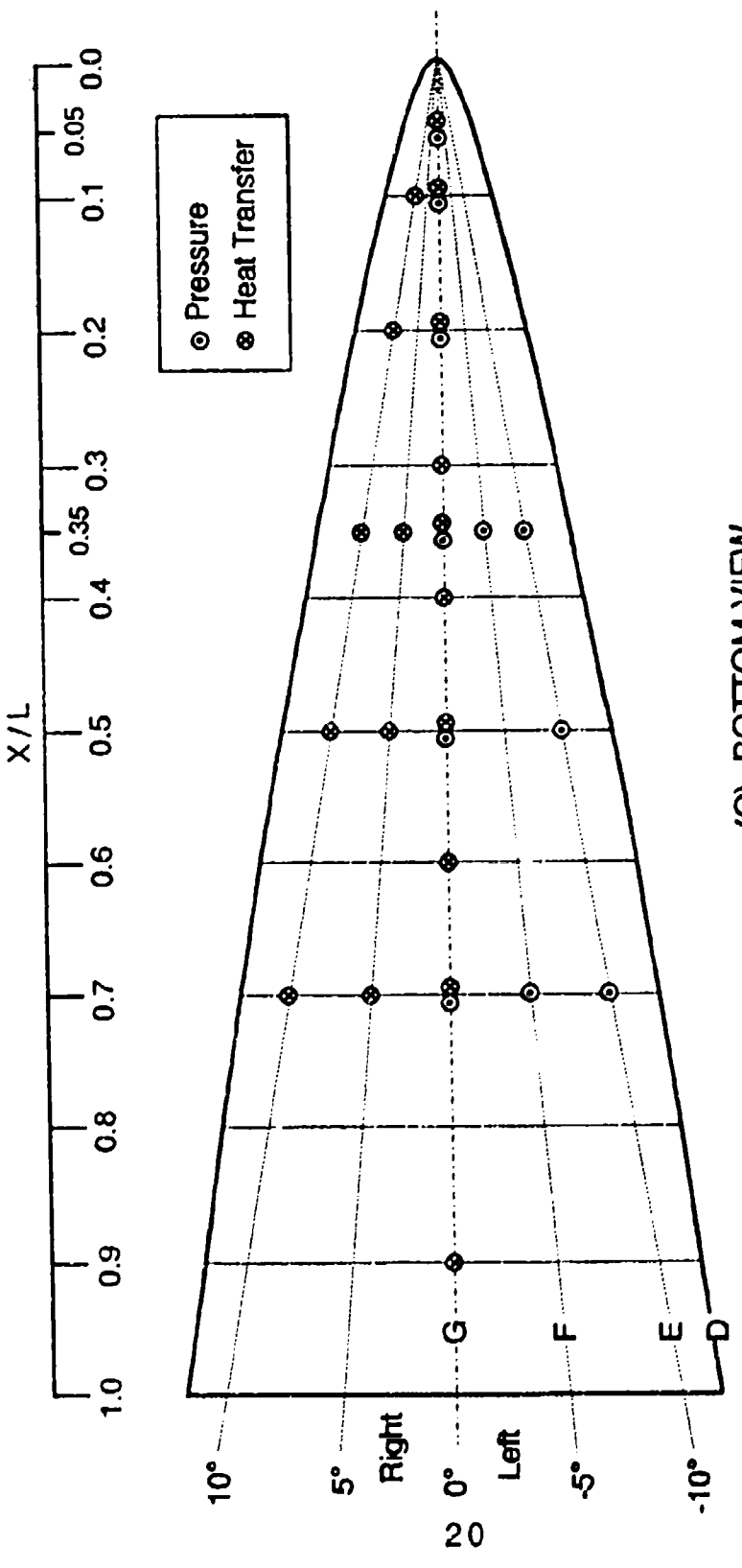

(C) BOTTOM VIEW

FIGURE 5. INSTRUMENTATION LOCATIONS (CONTINUED)

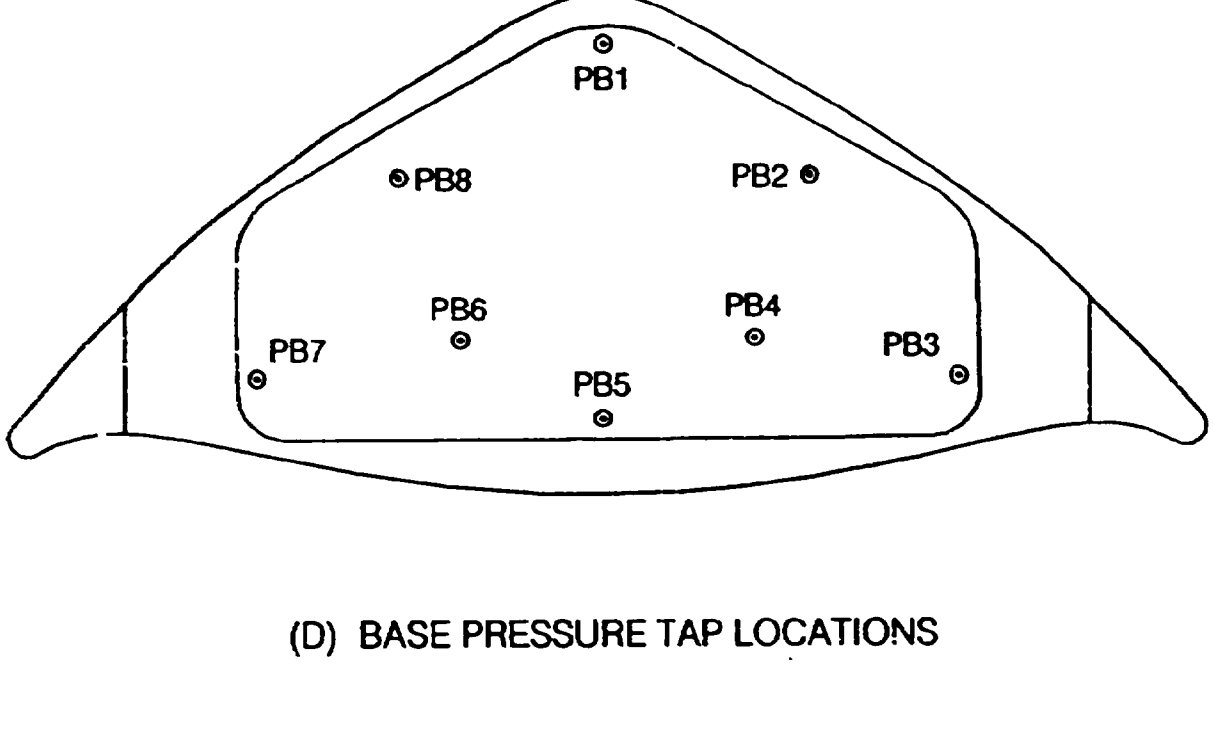

(D) BASE PRESSURE TAP LOCATIONS

FIGURE 5. INSTRUMENTATION LOCATIONS (CONTINUED)

FIGURE 6. 70-mm COLOR SCHLIEREN FLOW-VISUALIZATION PHOTOGRAPH FROM RUN 2388

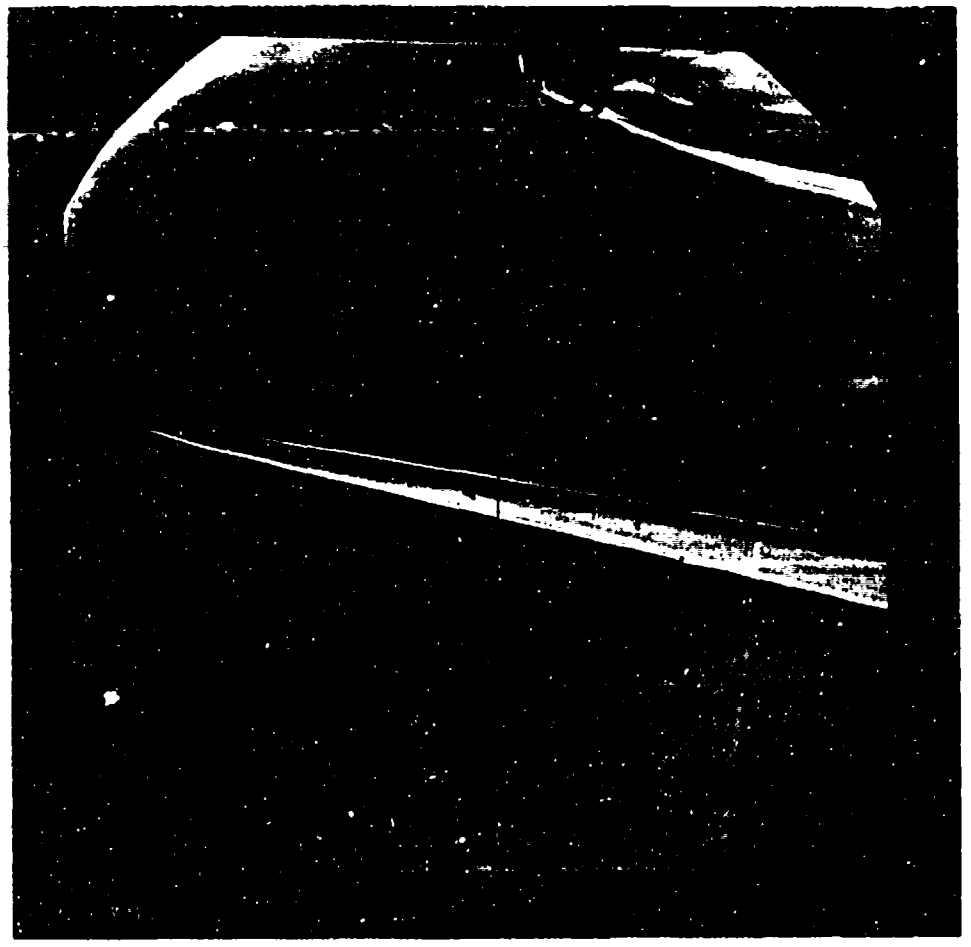

FIGURE 7. 70-mm COLOR SCHLIEREN FLOW-VISUALIZATION PHOTOGRAPH FROM RUN 2391

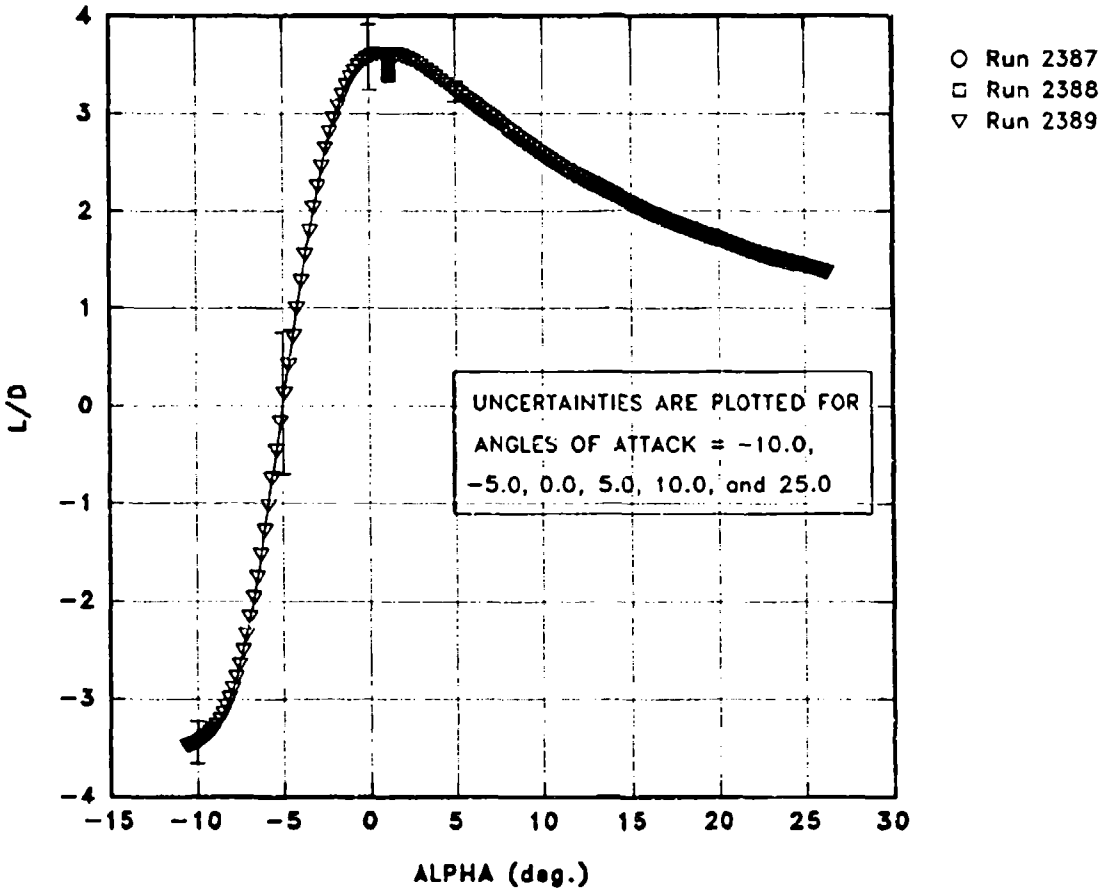

FIGURE 8. L/D VS. ALPHA FOR DESIGN CONDITION

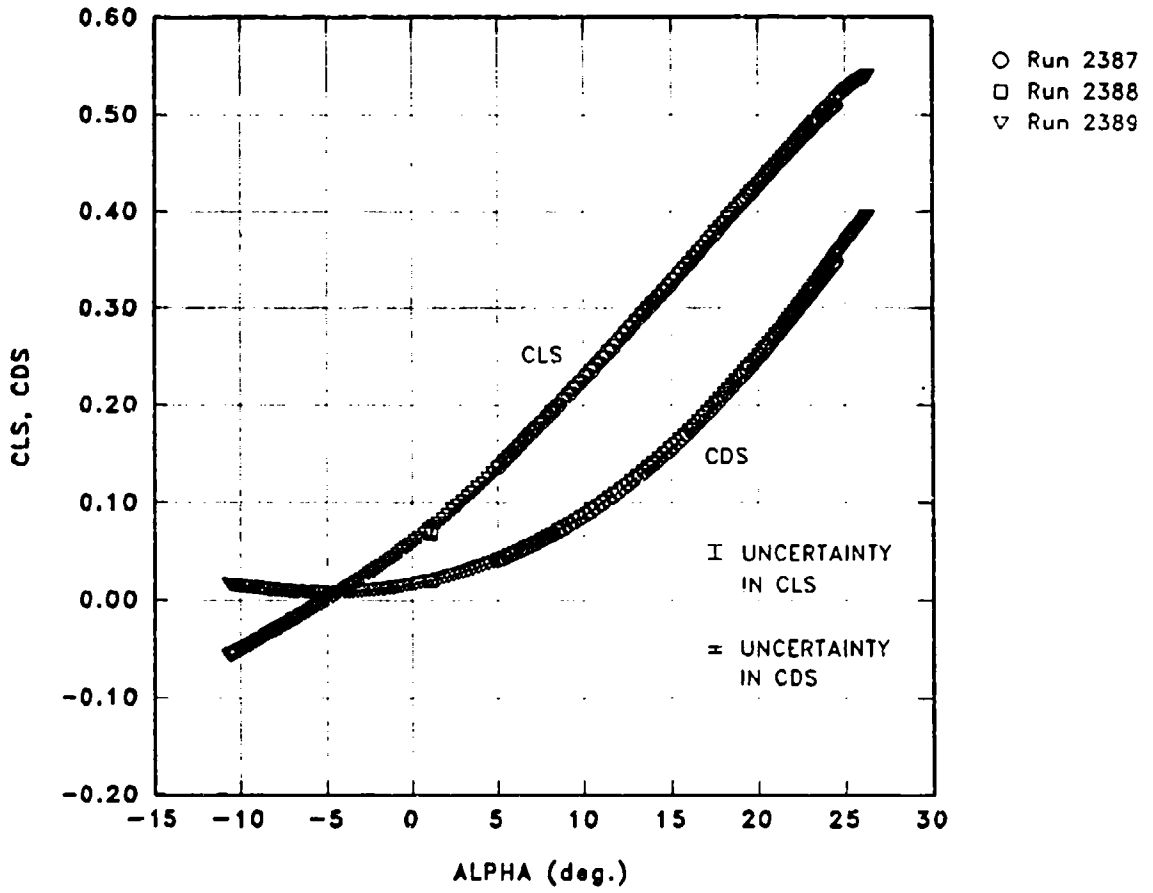

FIGURE 9. CLS, CDS VS. ALPHA FOR DESIGN CONDITION

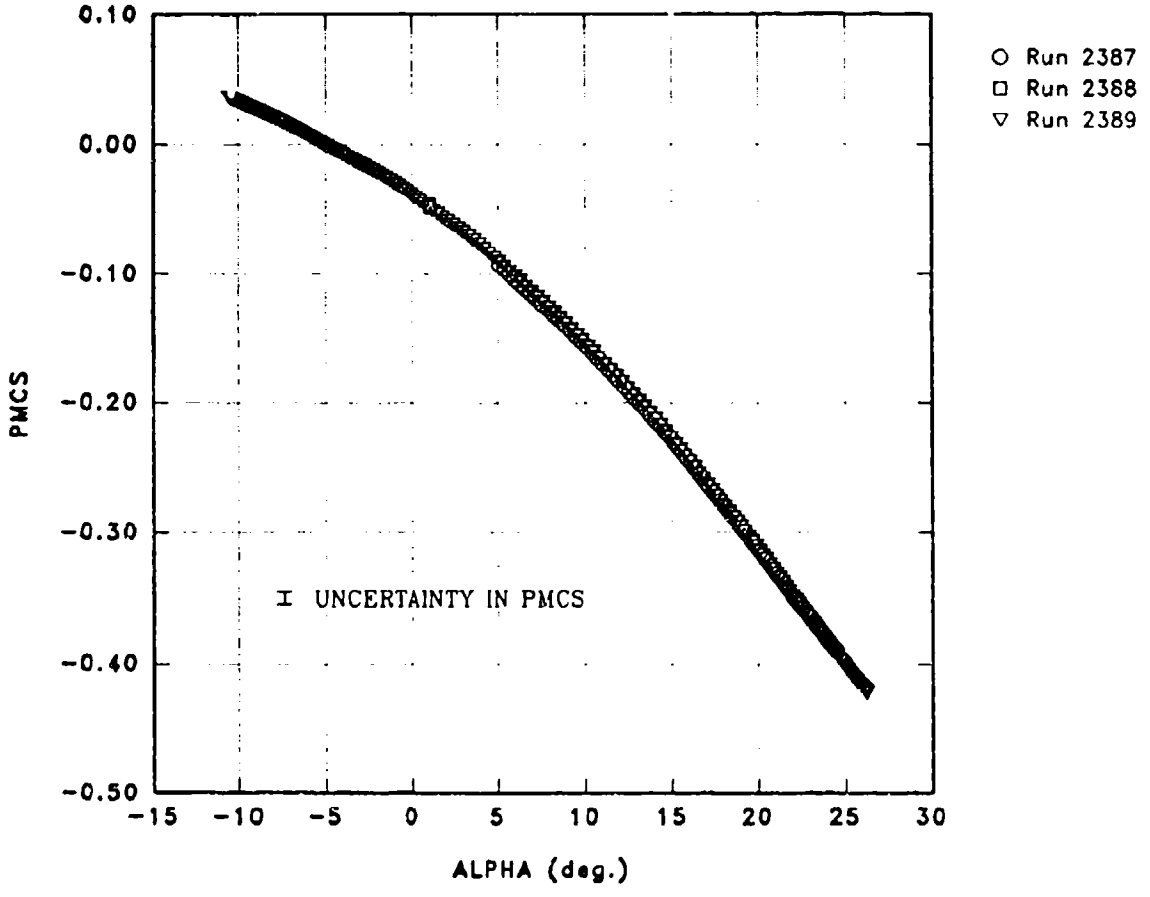

FIGURE 10. PMCS VS. ALPHA FOR DESIGN CONDITION

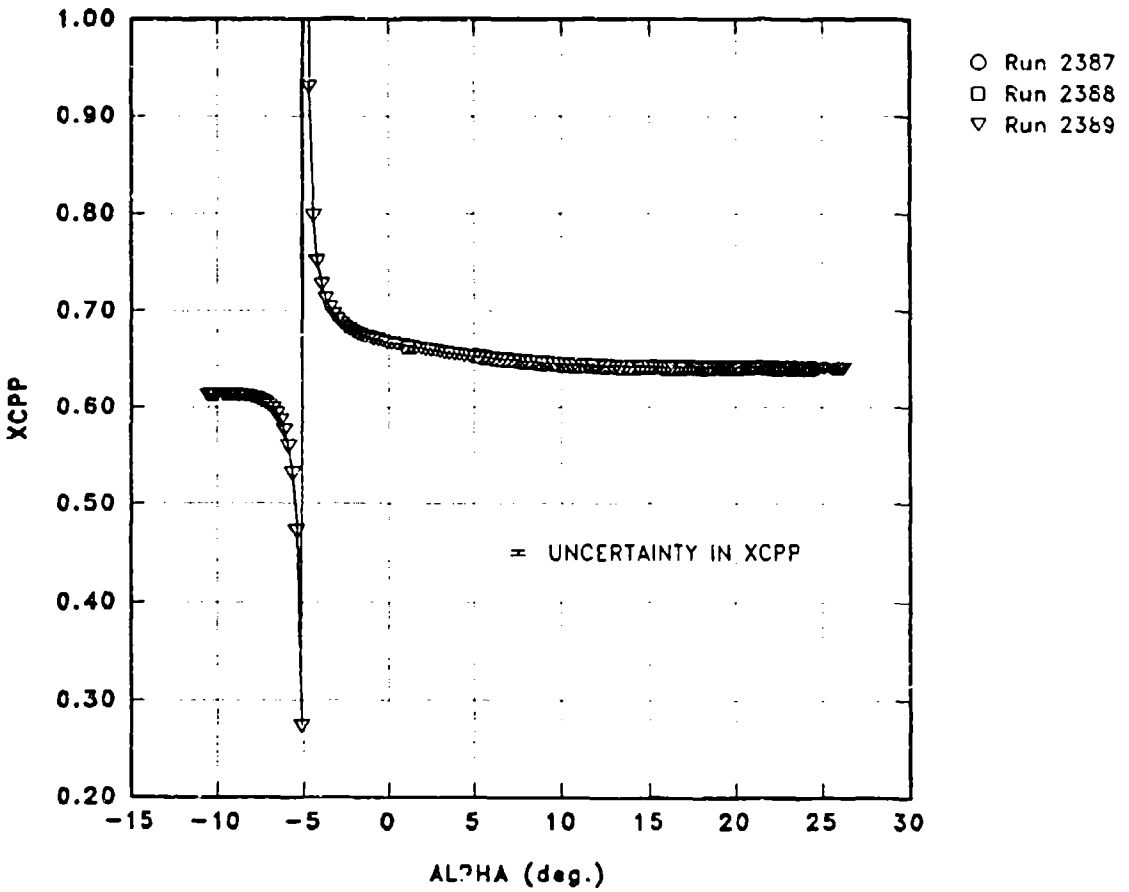

FIGURE 11. XCPP VS. ALPHA FOR DESIGN CONDITION

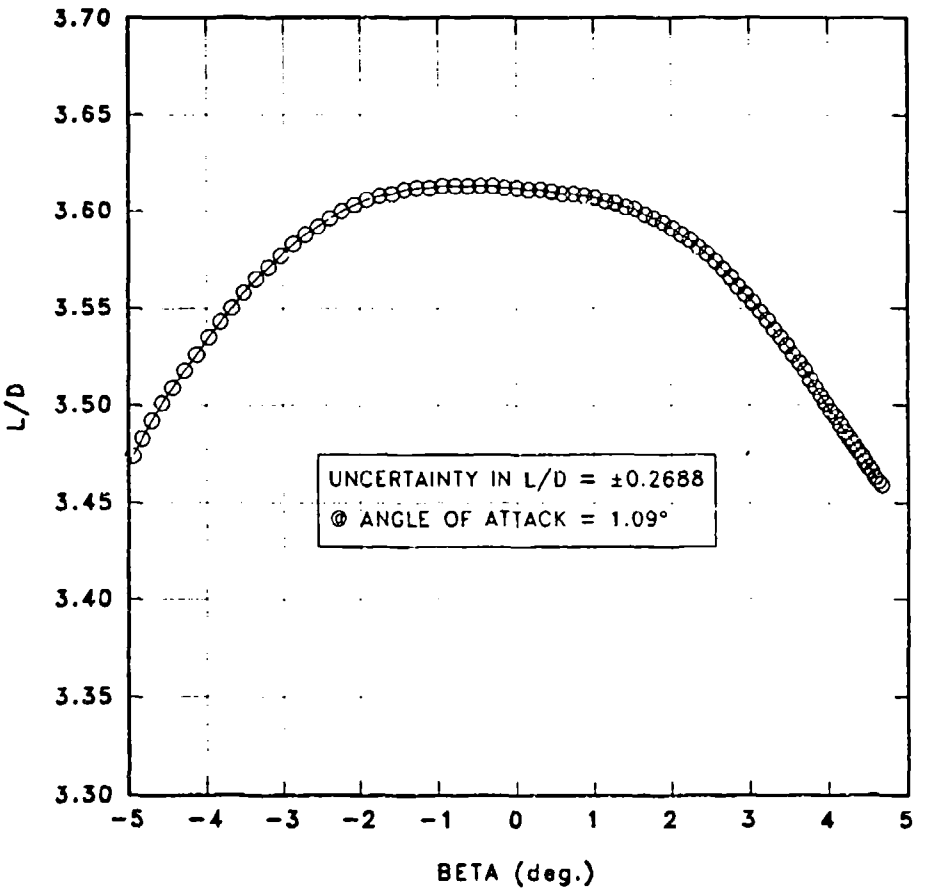

FIGURE 12. L/D VS. BETA FOR DESIGN CONDITION

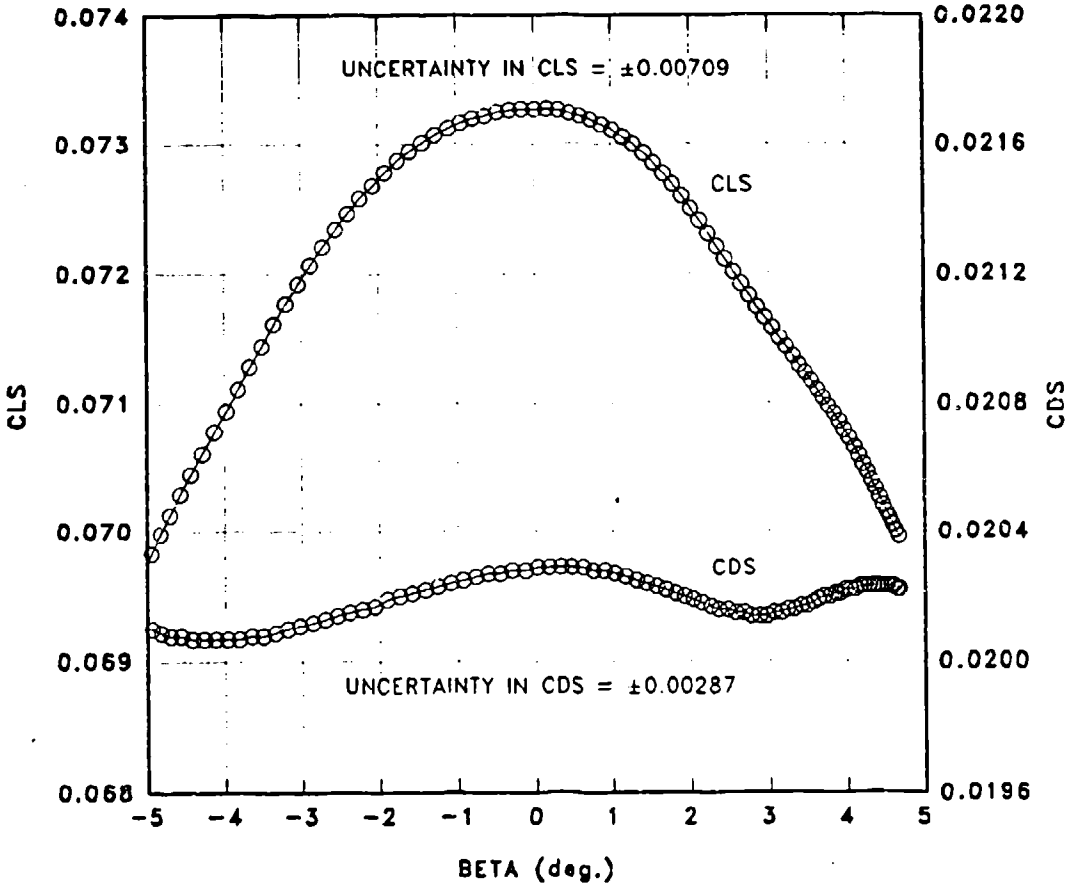

FIGURE 13. CLS, CDS VS. BETA FOR DESIGN CONDITION

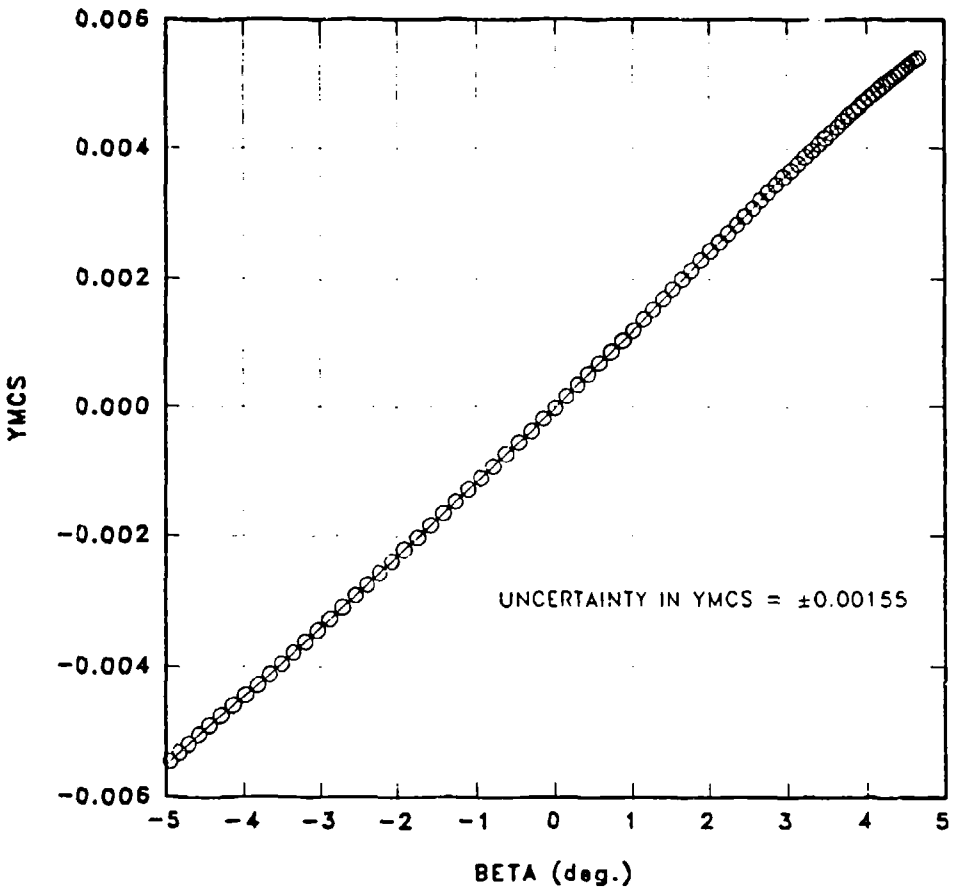

FIGURE 14. YMCS VS. BETA FOR DESIGN CONDITION

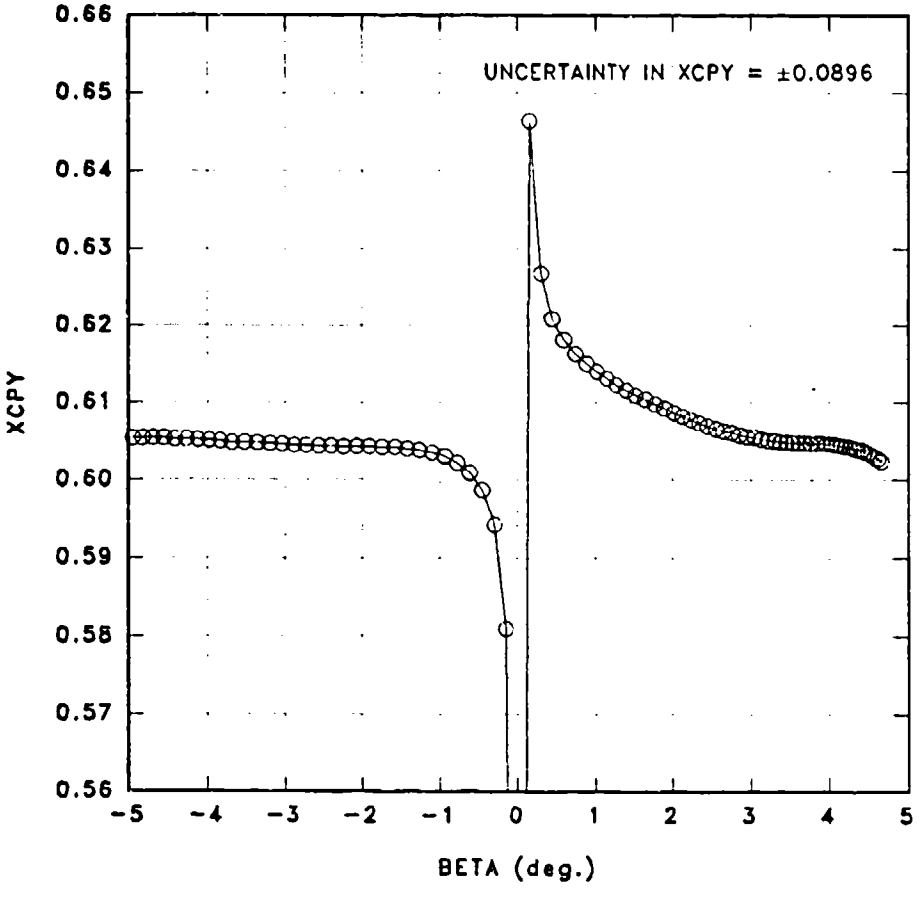

FIGURE 15. XCPY VS. BETA FOR DESIGN CONDITION

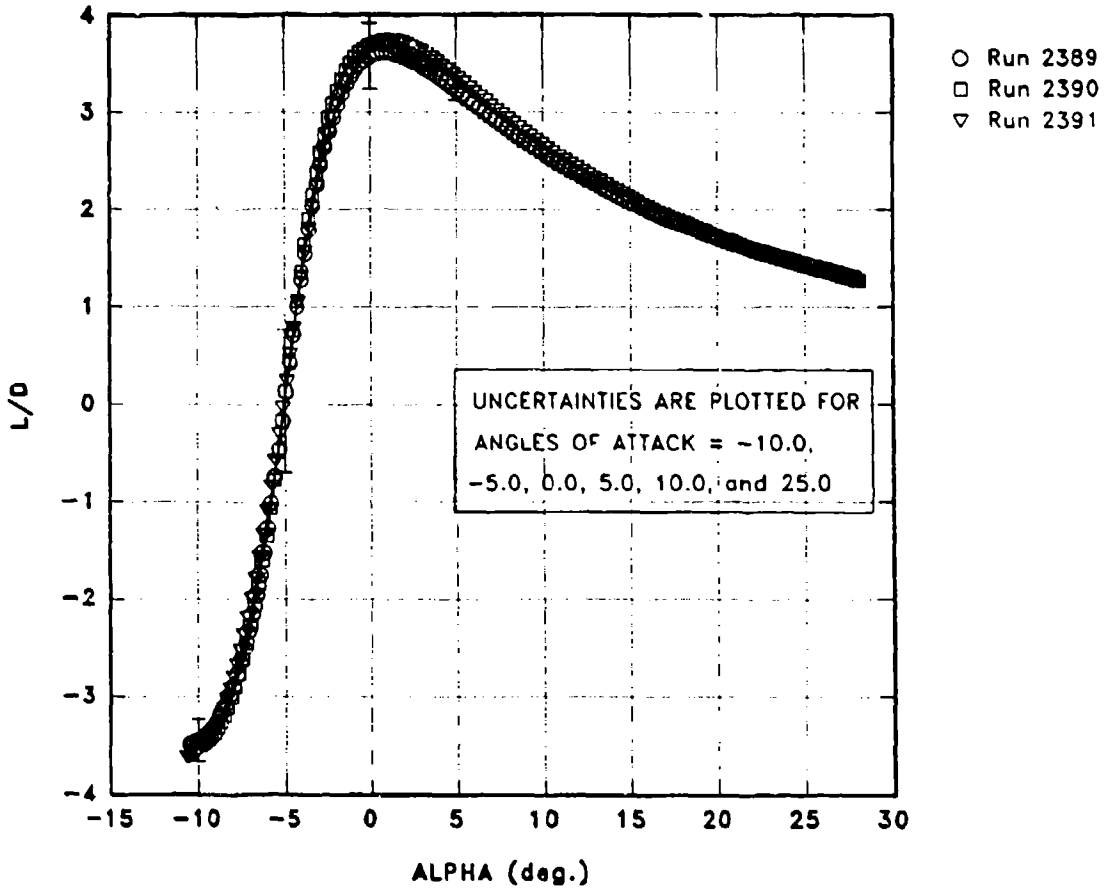

FIGURE 16. MACH-NUMBER EFFECTS ON L/D VS. ALPHA

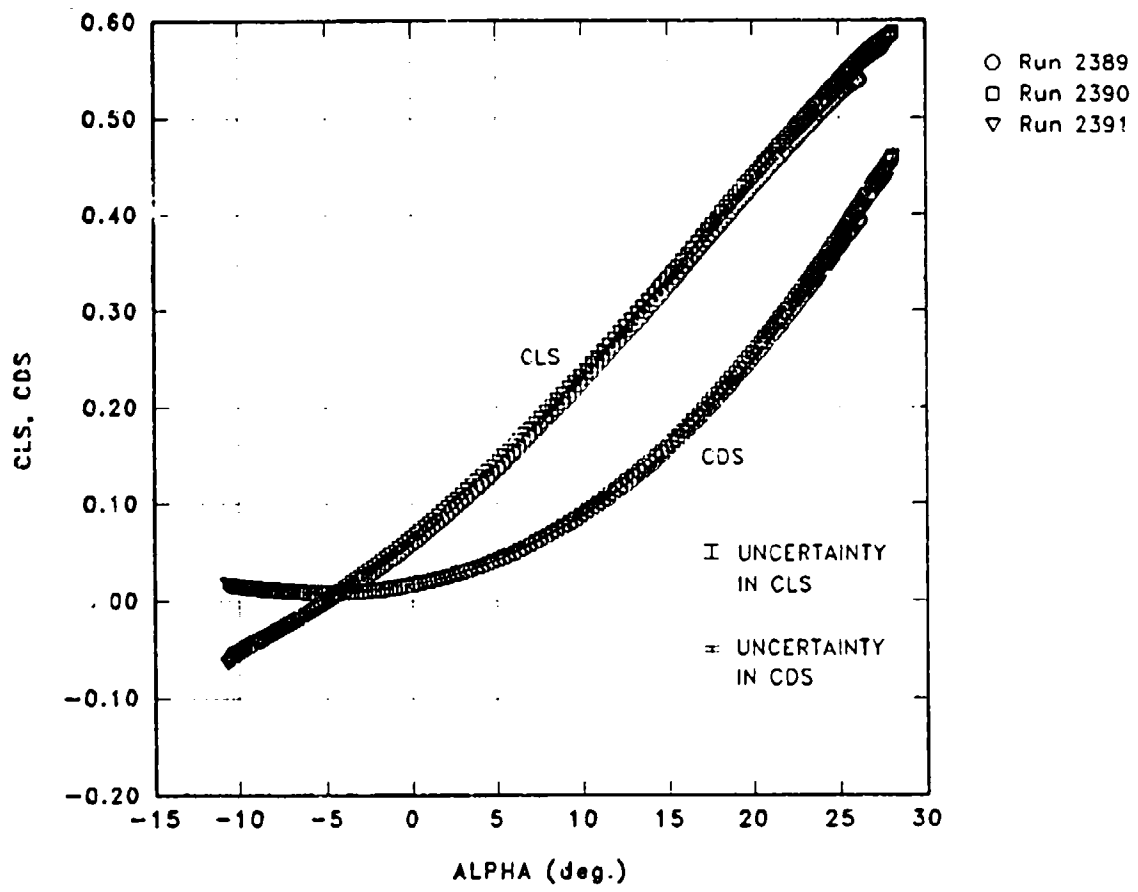

FIGURE 17. MACH-NUMBER EFFECTS ON CLS, CDS VS. ALPHA

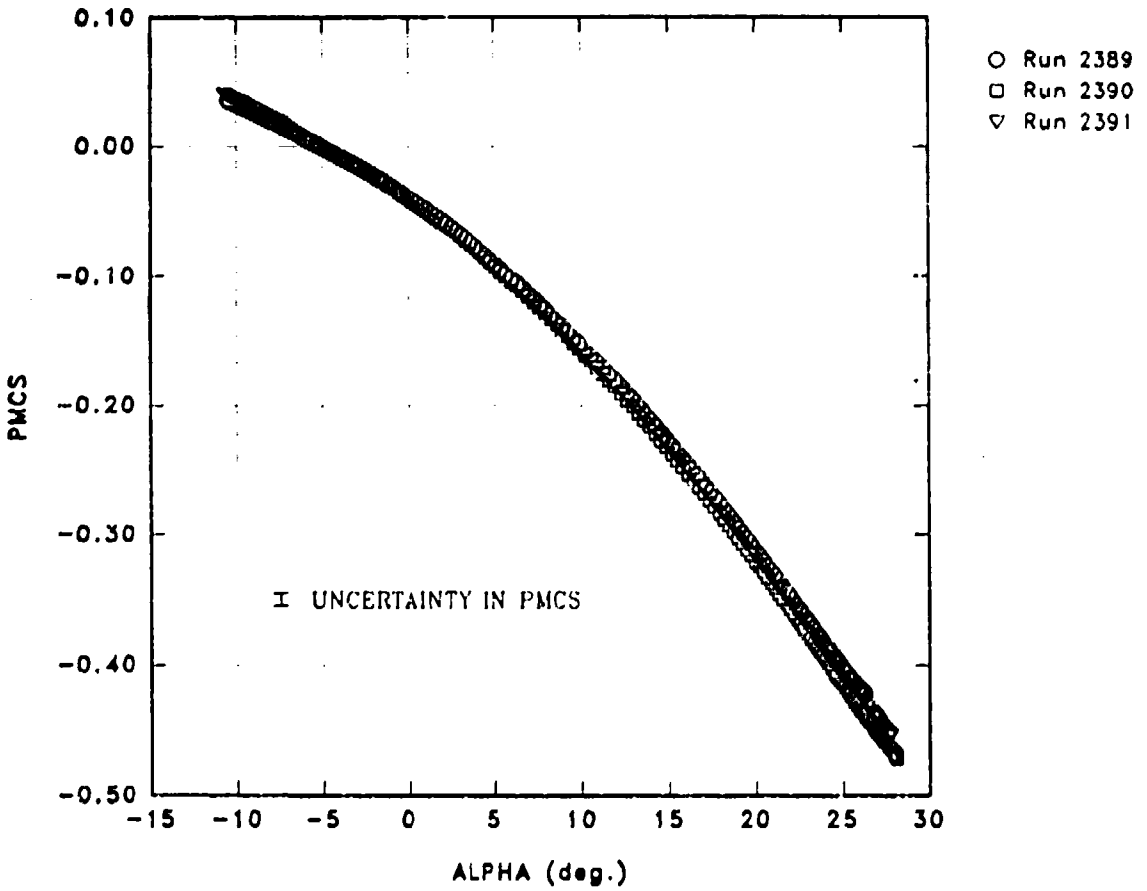

FIGURE 18. MACH-NUMBER EFFECTS ON PMCS VS. ALPHA

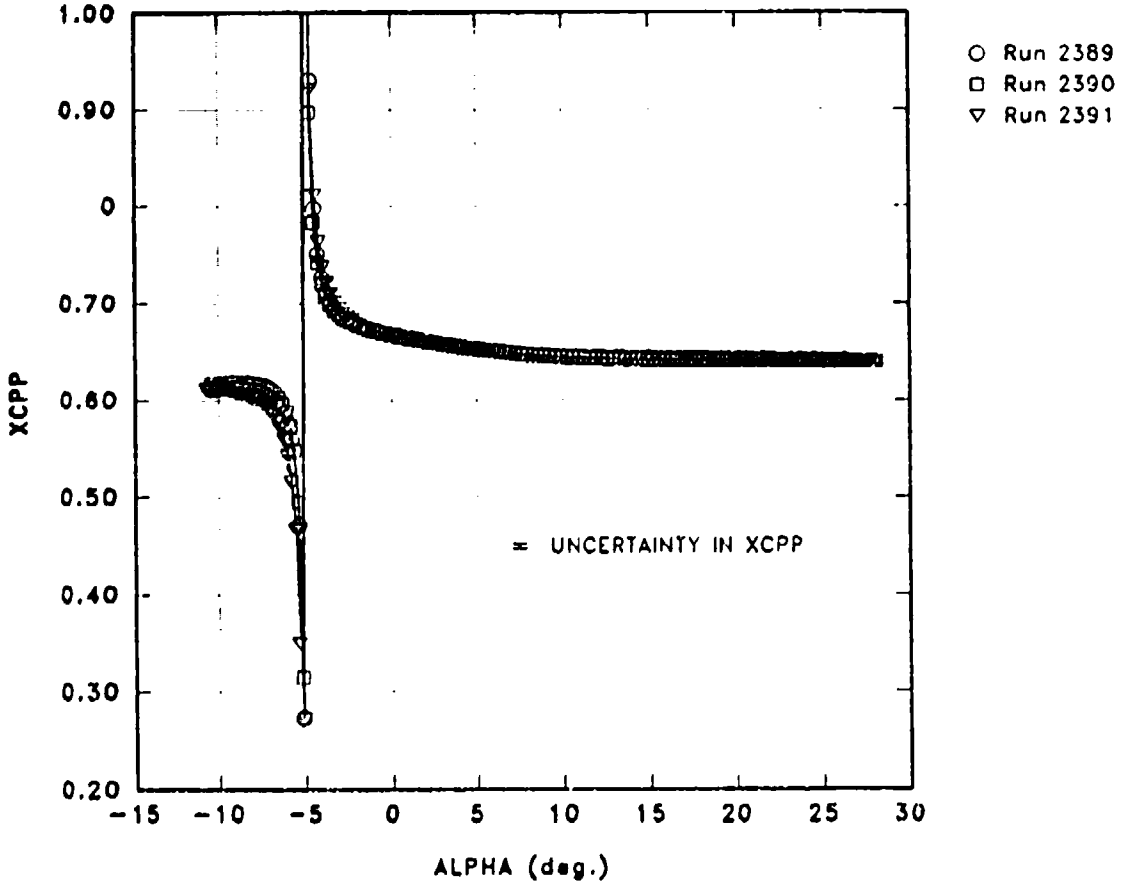

FIGURE 19. MACH-N MBER EFFECTS ON XCPP VS. ALPHA

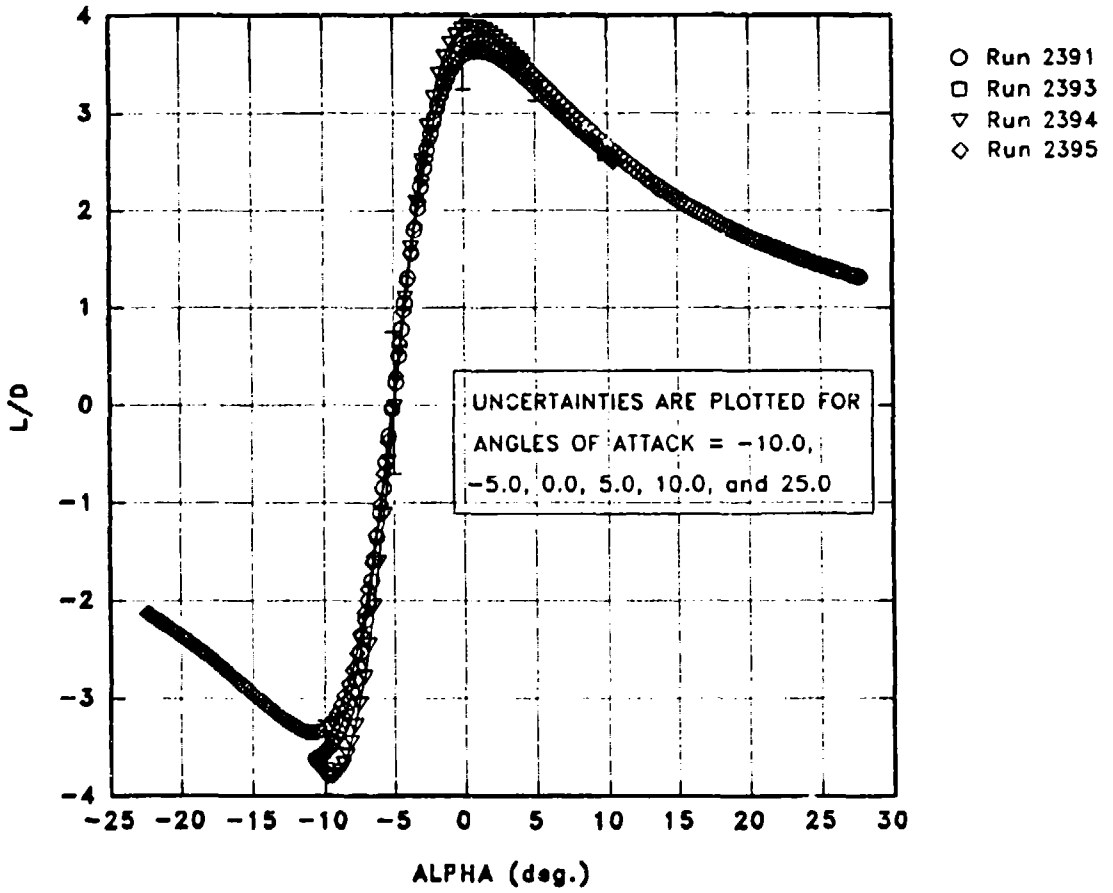

FIGURE 20. REYNOLDS-NUMBER EFFECTS ON L/D VS. ALPHA

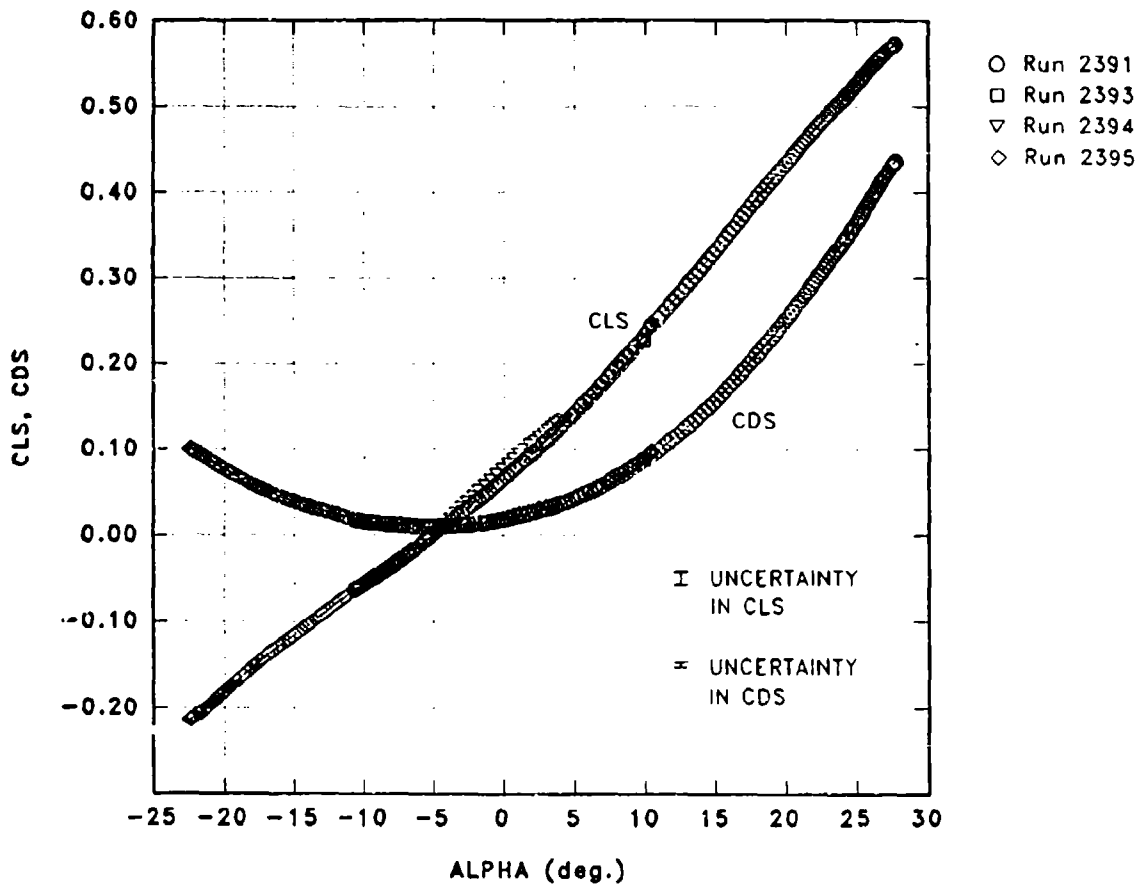

FIGURE 21. REYNOLDS-NUMBER EFFECTS ON CLS, CDS VS. ALPHA

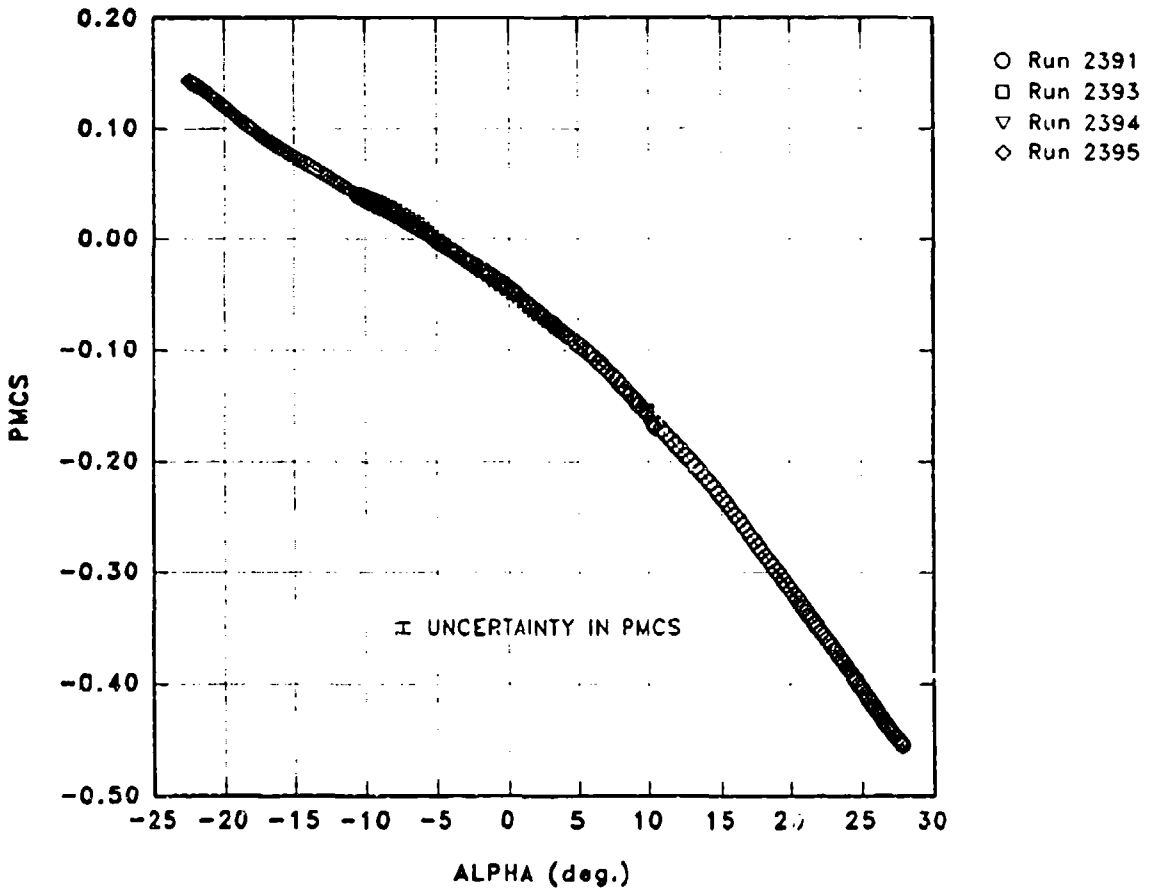

FIGURE 22. REYNOLDS-NUMBER EFFECTS ON PMCS VS. ALPHA

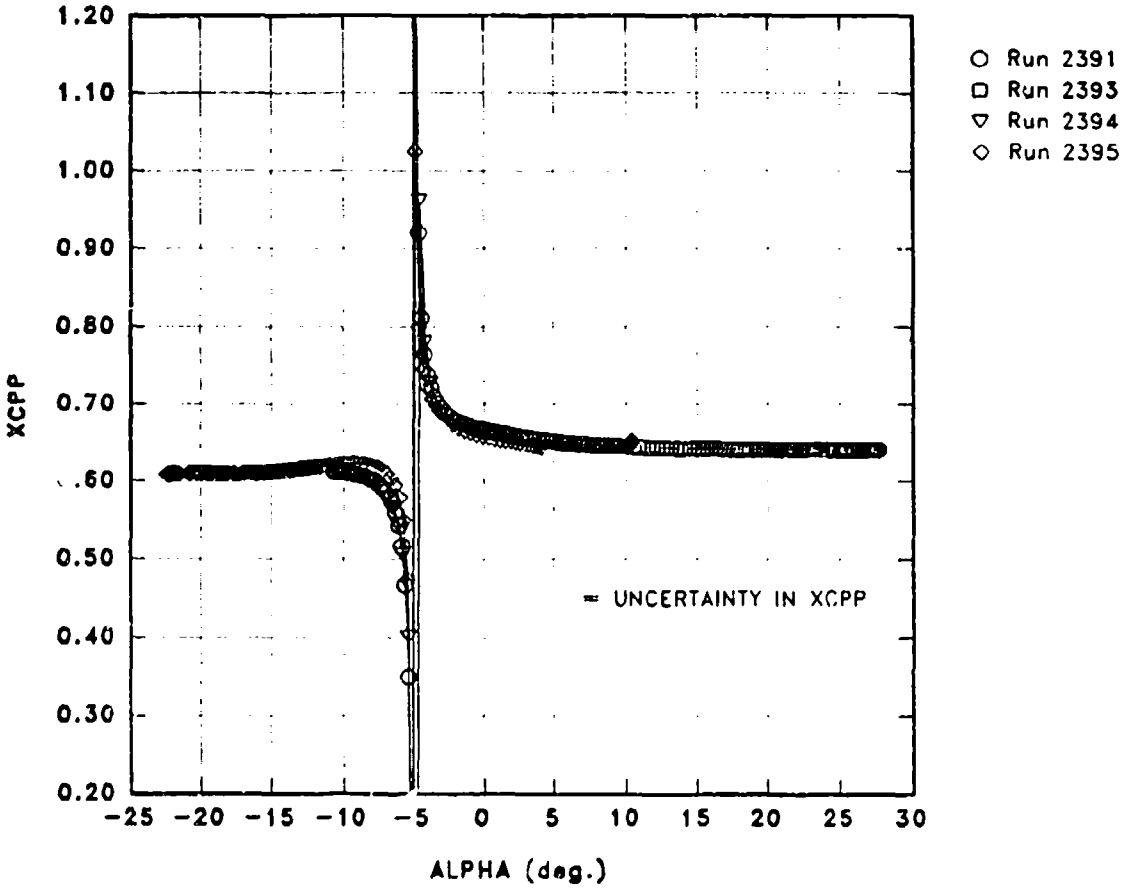

FIGURE 23. REYNOLDS-NUMBER EFFECTS ON XCPP VS. ALPHA

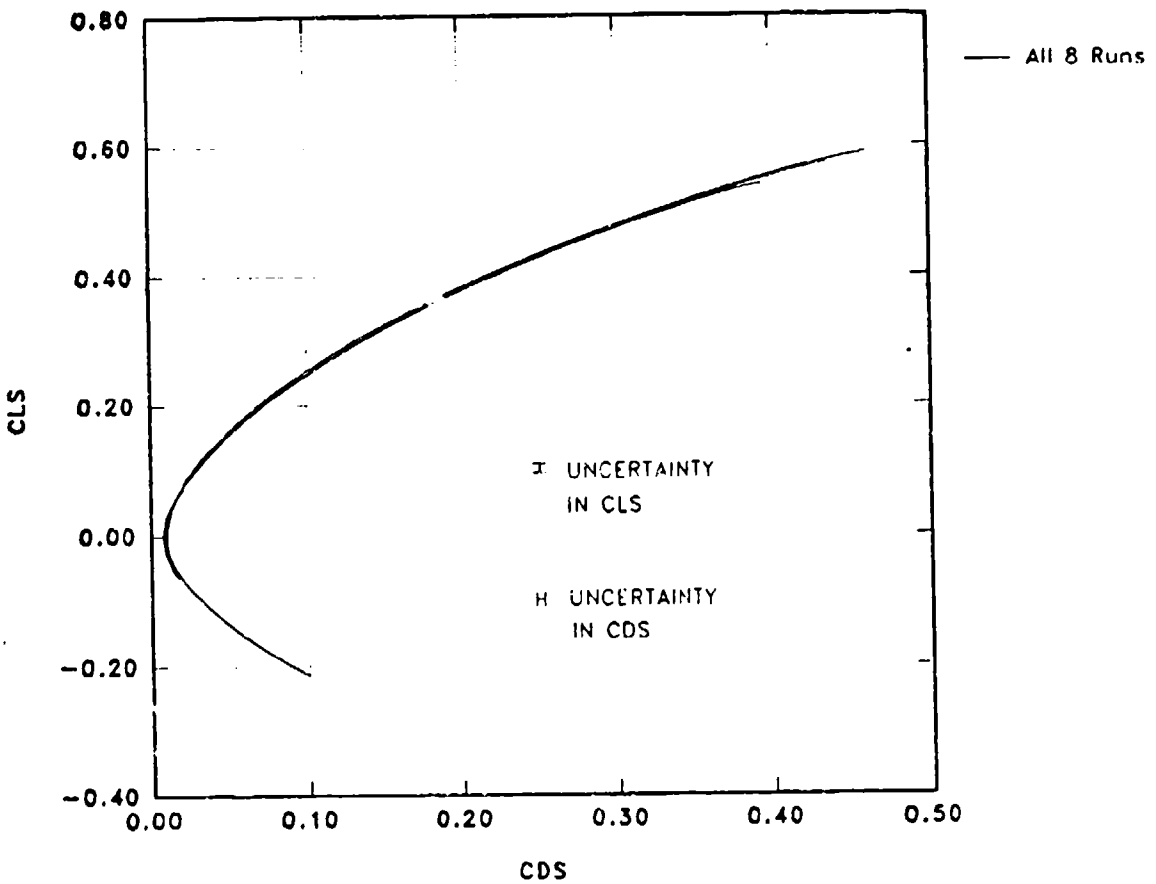

FIGURE 24. DRAG POLAR, CLS VS. CDS, FOR ALL RUNS

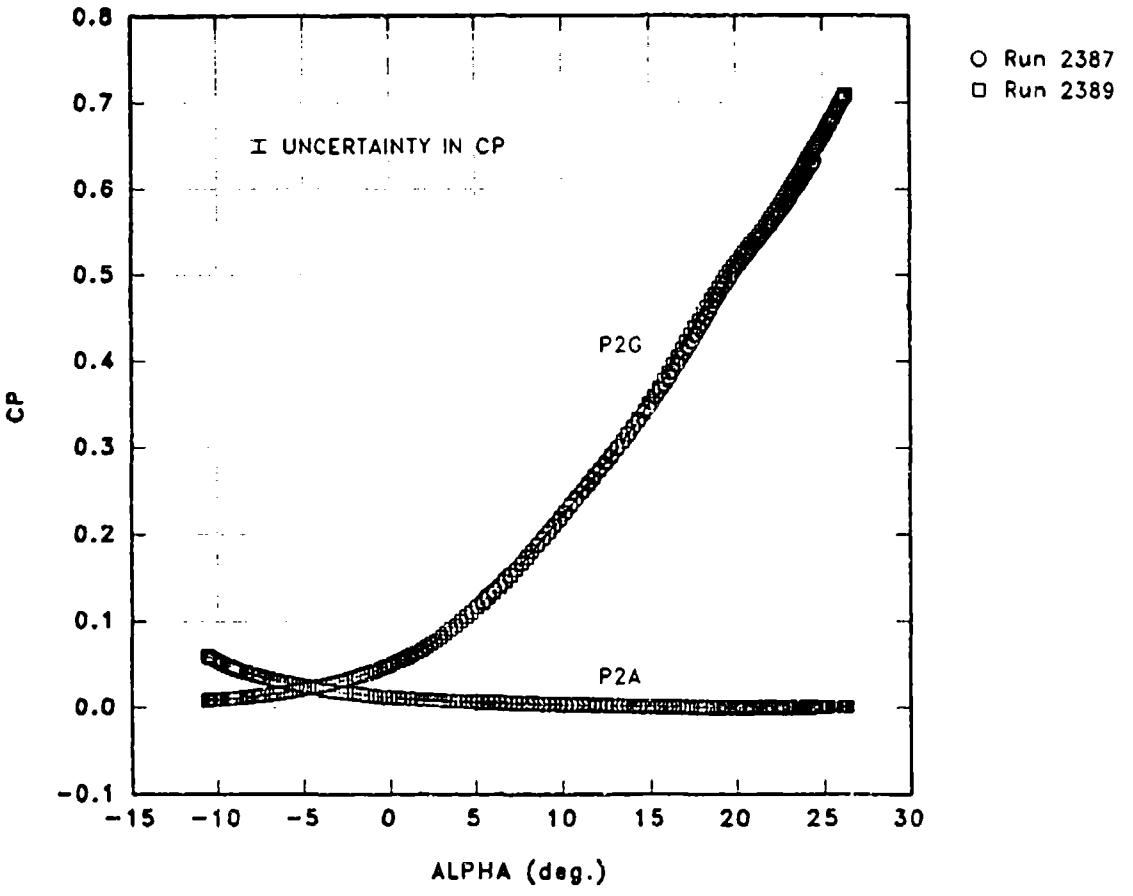

FIGURE 25. PRESSURE COEFFICIENT VS. ALPHA FOR DESIGN CONDITION

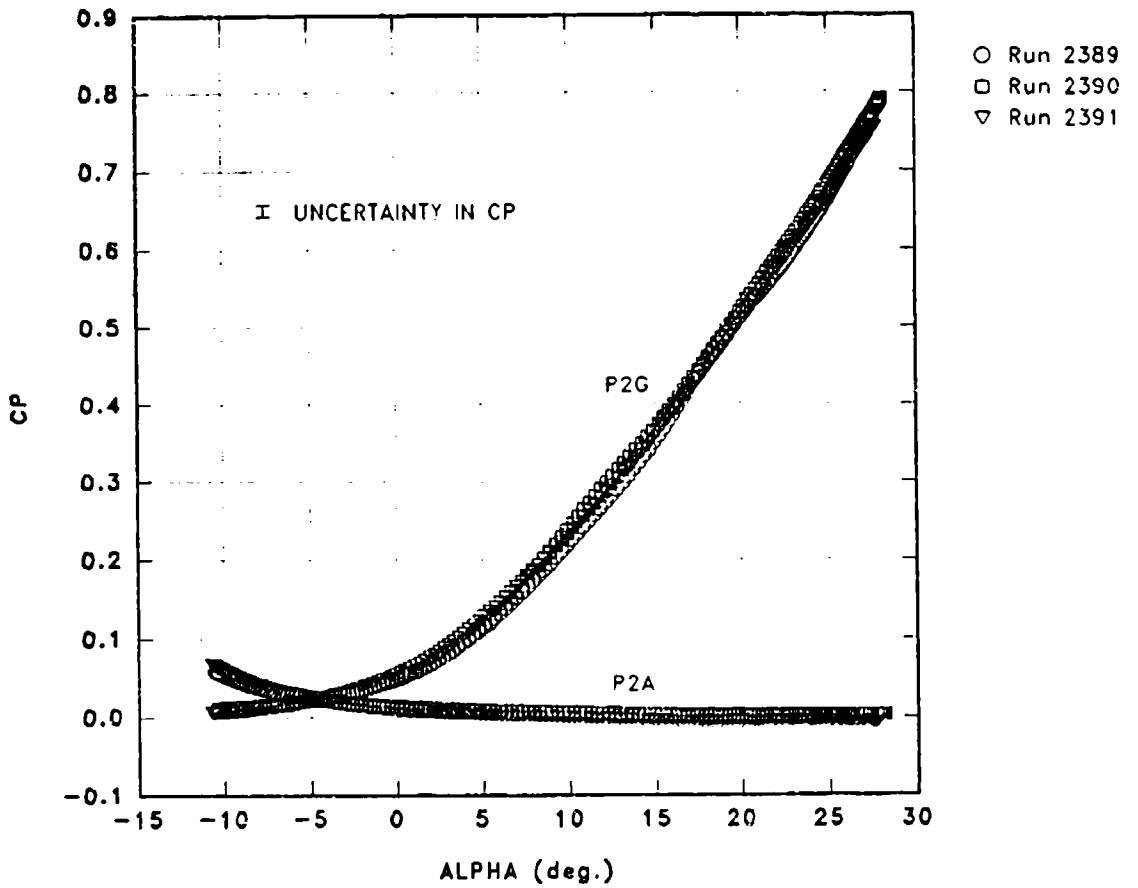

FIGURE 26. MACH-NUMBER EFFECTS ON CP VS. ALPHA

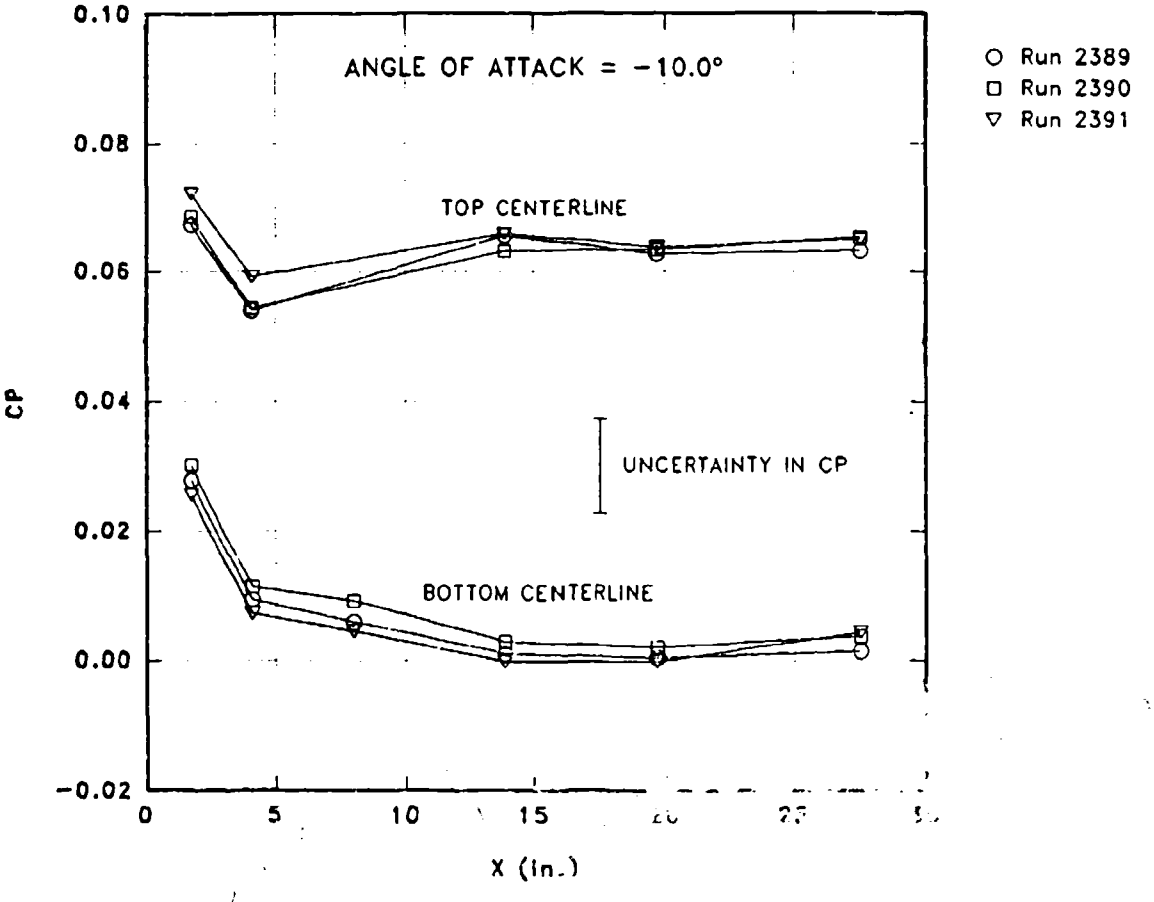

FIGURE 27. AXIAL VARIATIONS IN CP FOR ALPHA = -10.0°

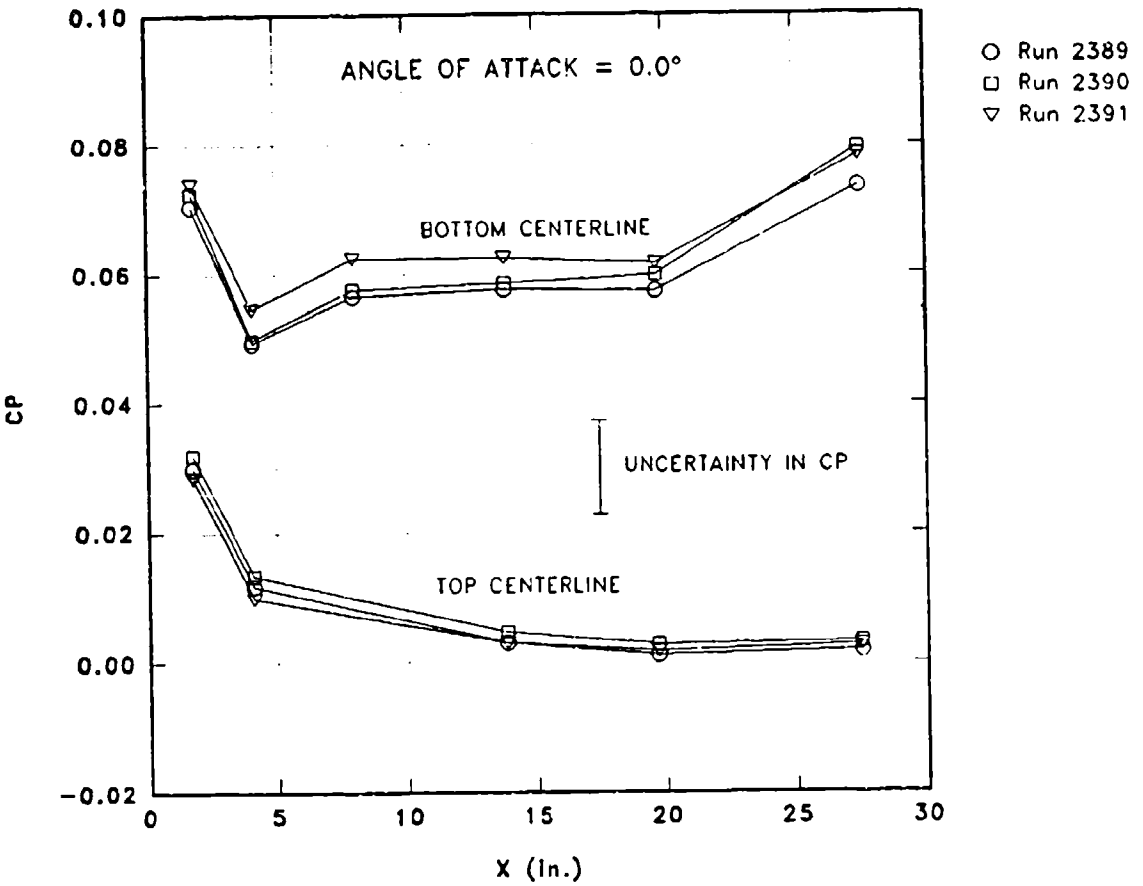

FIGURE 28. AXIAL VARIATIONS IN CP FOR ALPHA = 0.0°

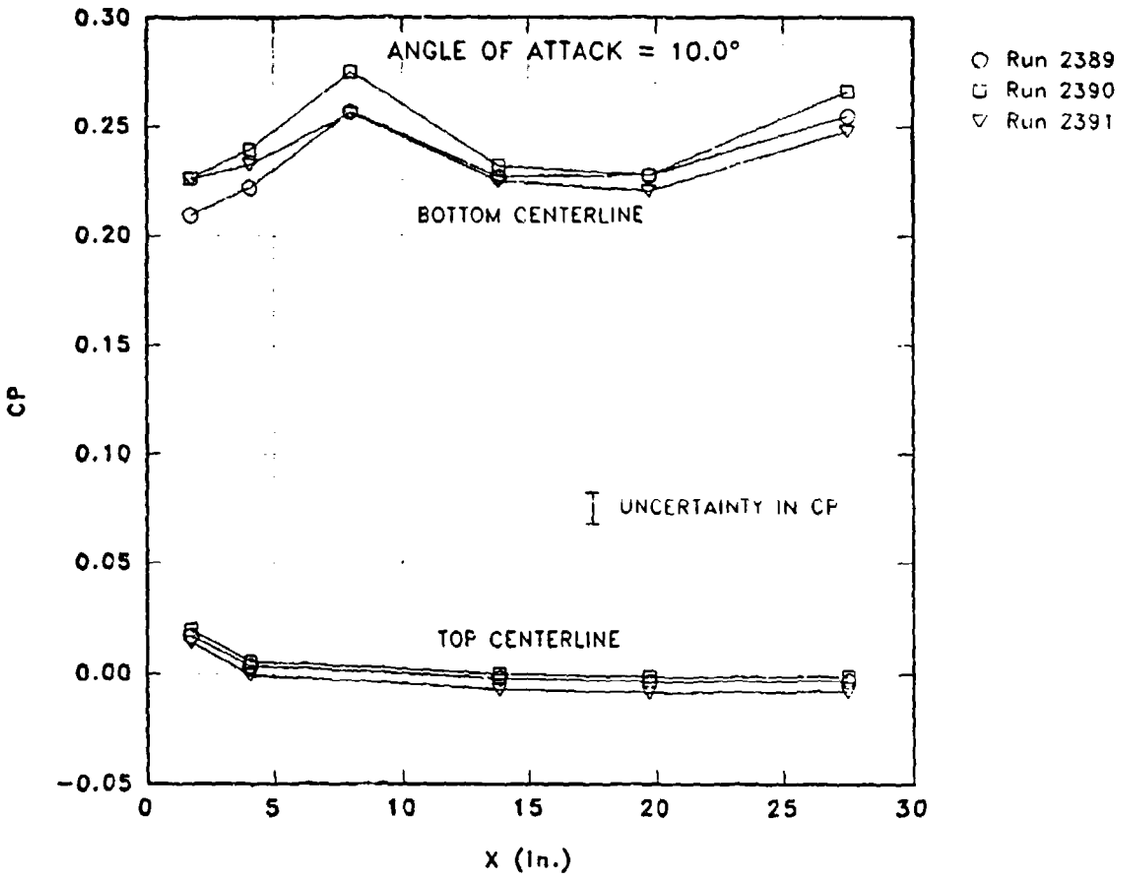

FIGURE 29. AXIAL VARIATIONS IN CP FOR ALPHA = 10.0°

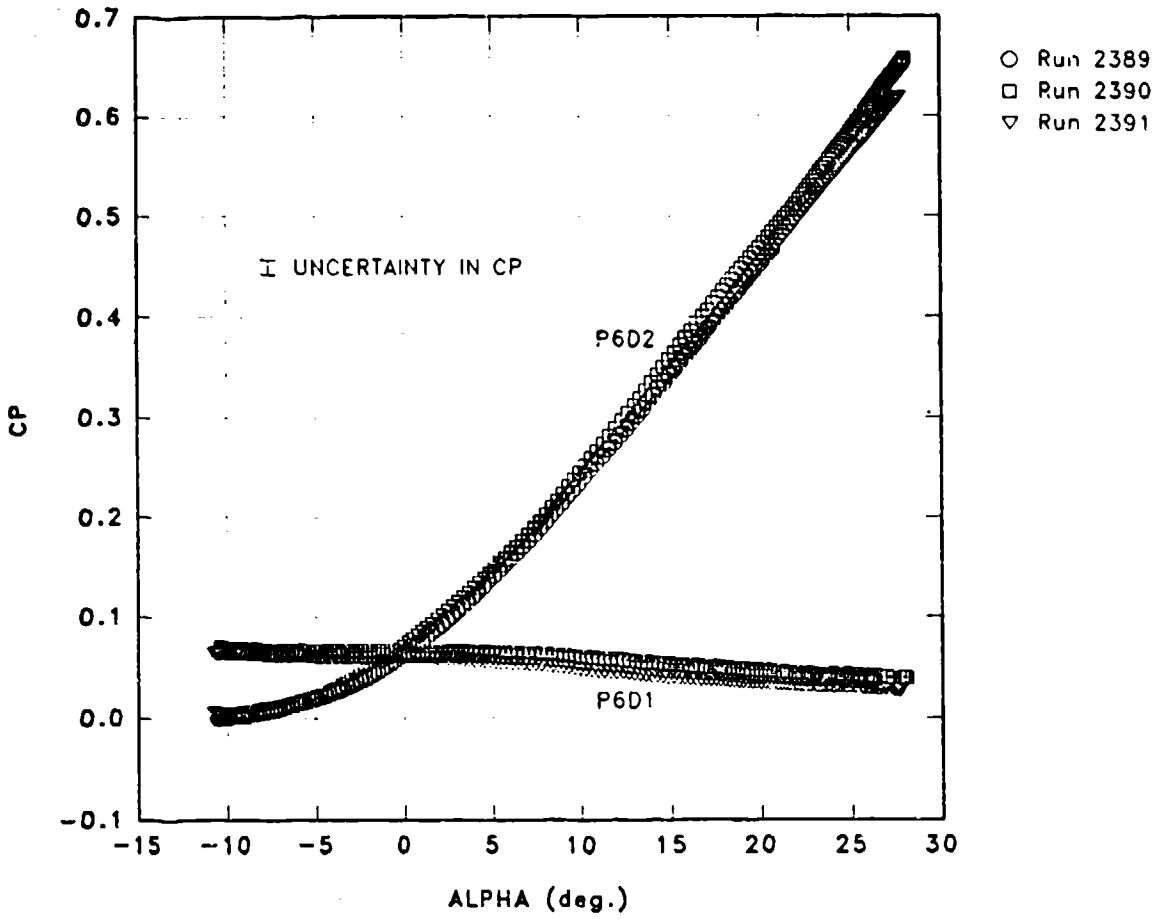

FIGURE 30. MACH-NUMBER EFFECTS ON LEADING-EDGE CP VS ALPHA

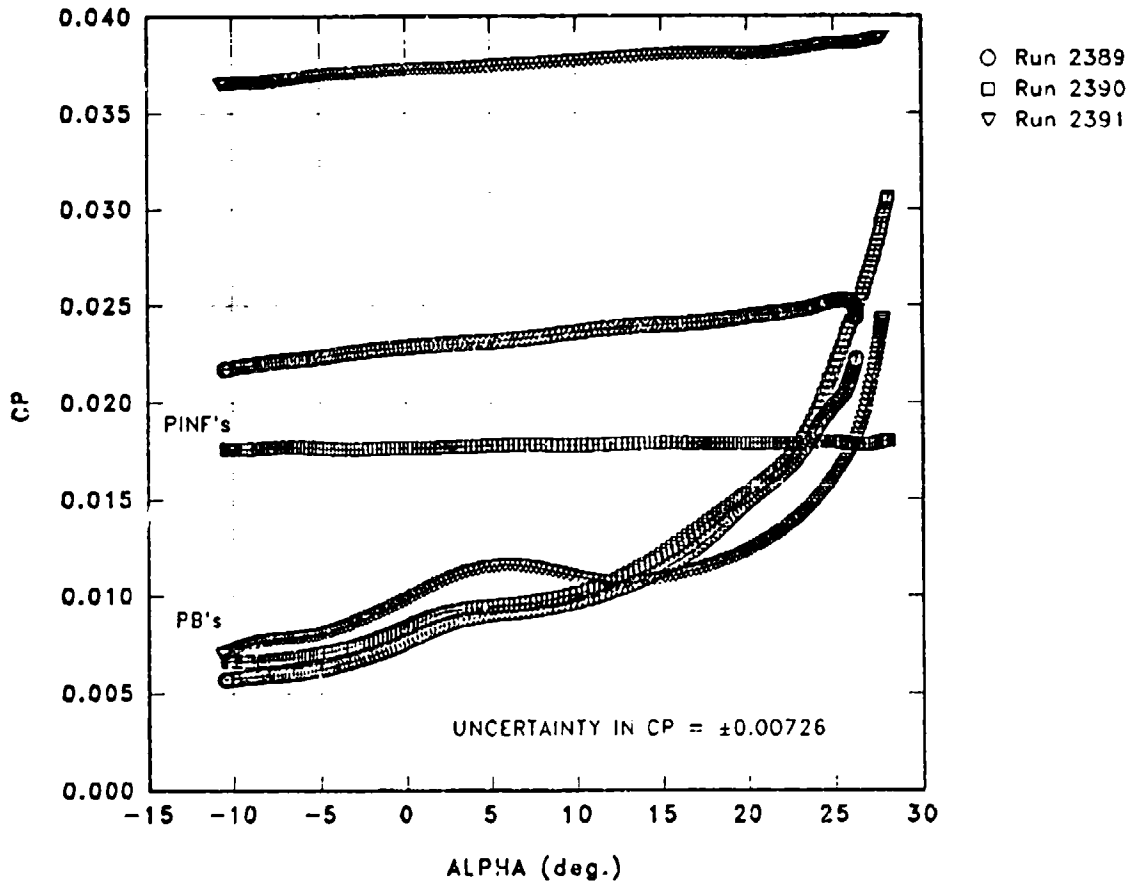

FIGURE 31. MACH-NUMBER EFFECTS ON BASE AND FREESTREAM CP'S

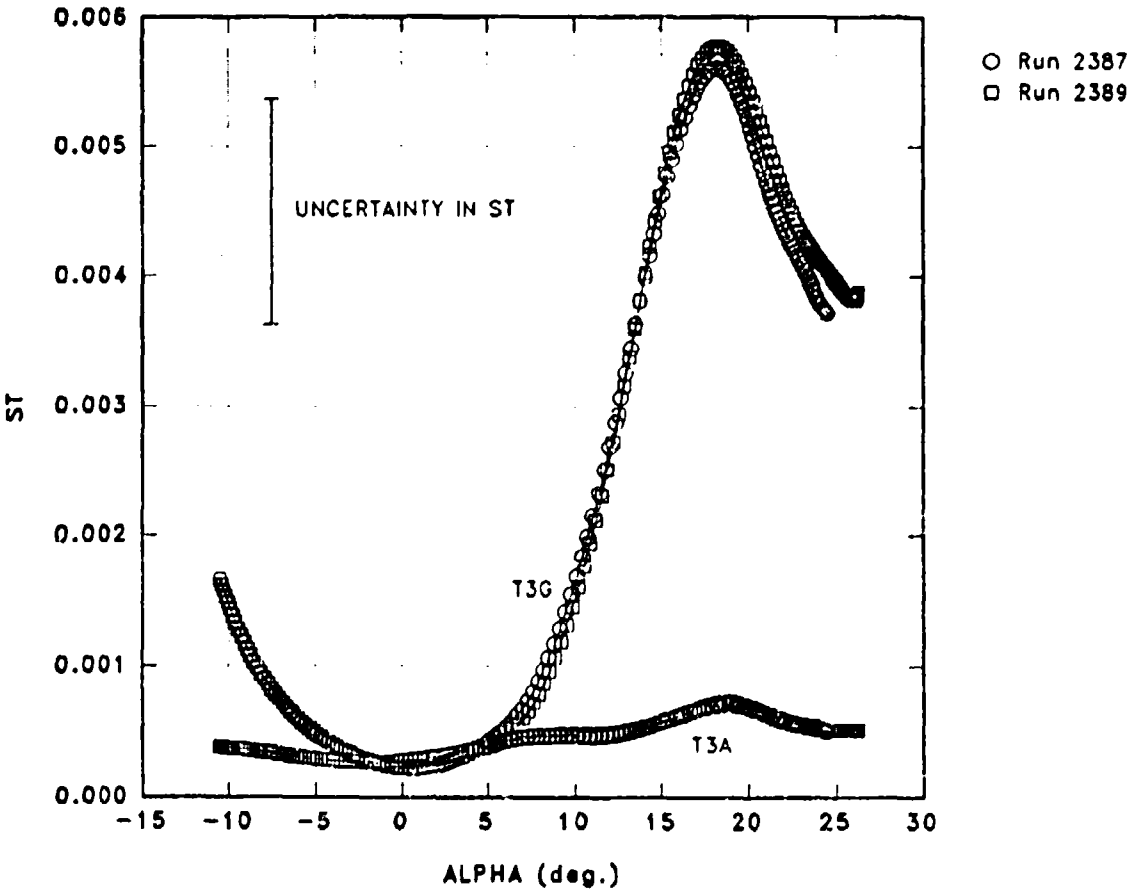

FIGURE 32. STANTON NUMBER VS. ALPHA FOR DESIGN CONDITION

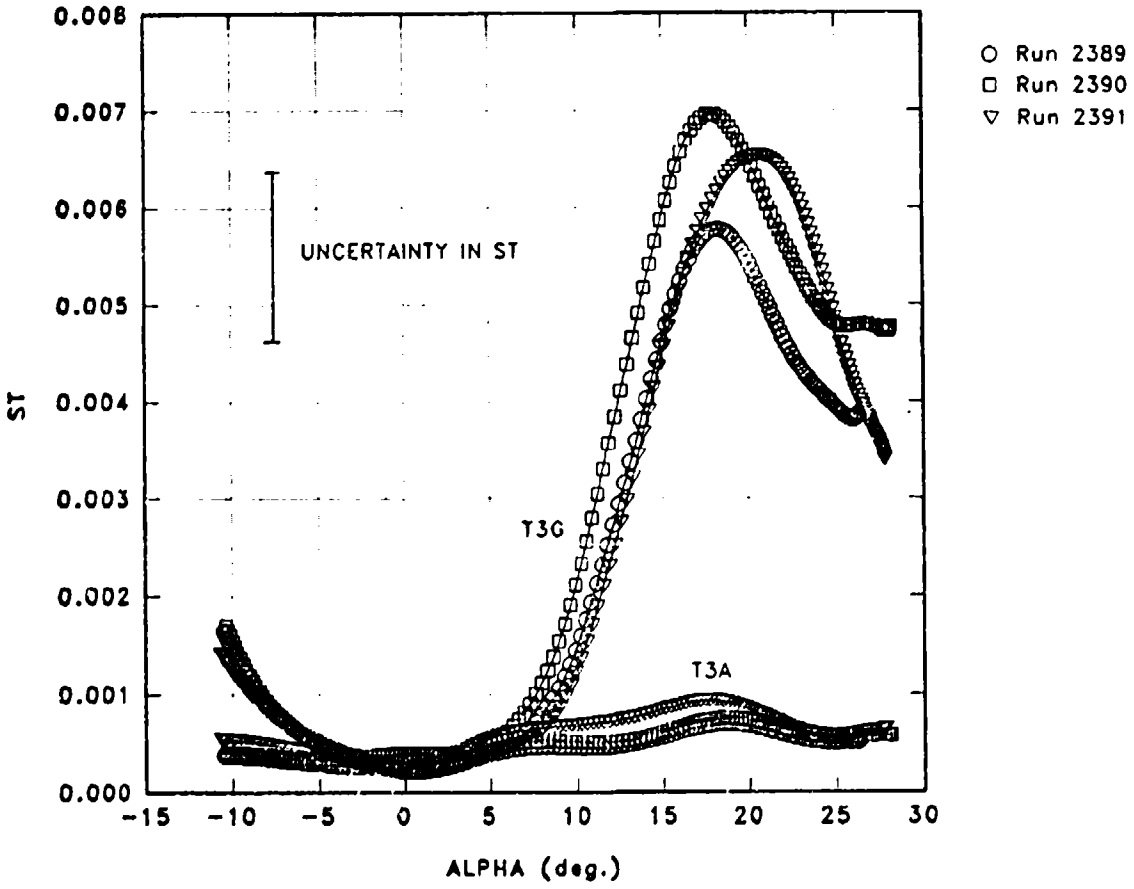

FIGURE 33. MACH-NUMBER EFFECTS ON ST VS. ALPHA

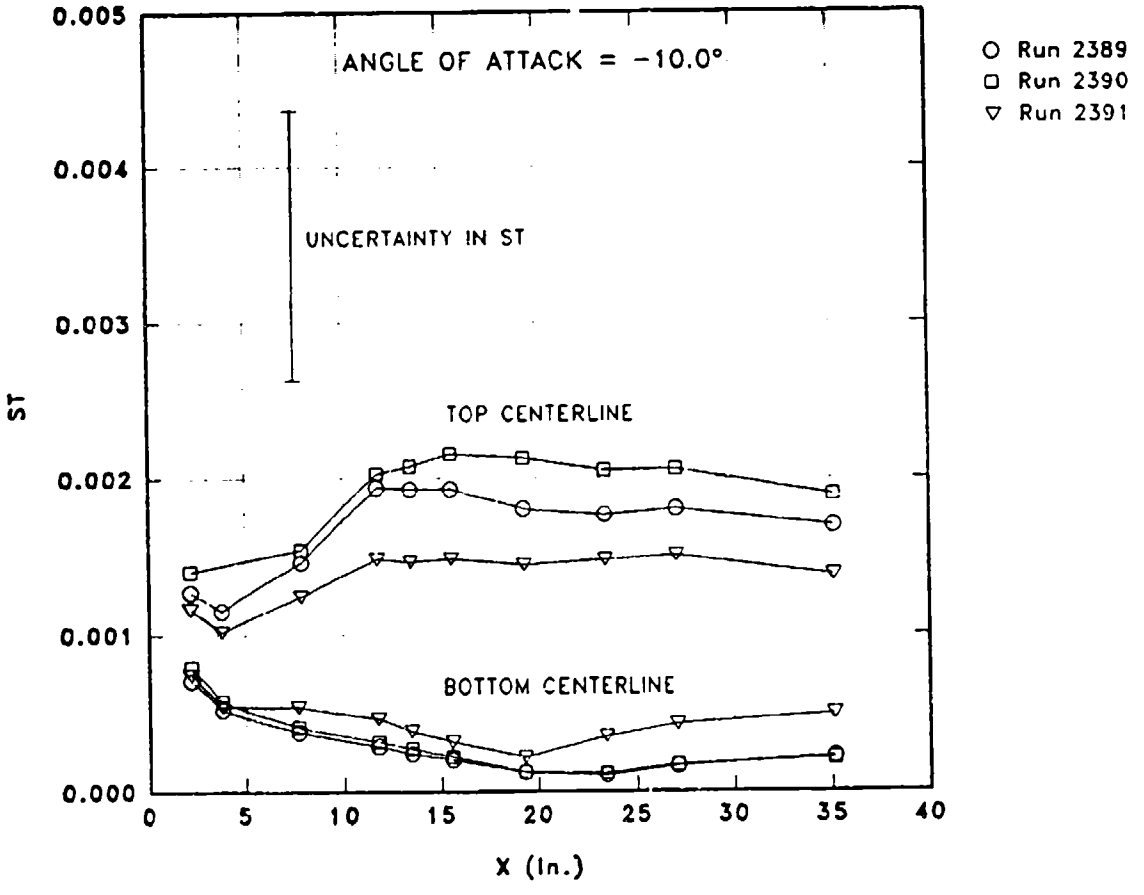

FIGURE 34. AXIAL VARIATIONS IN ST FOR ALPHA = -10.0°

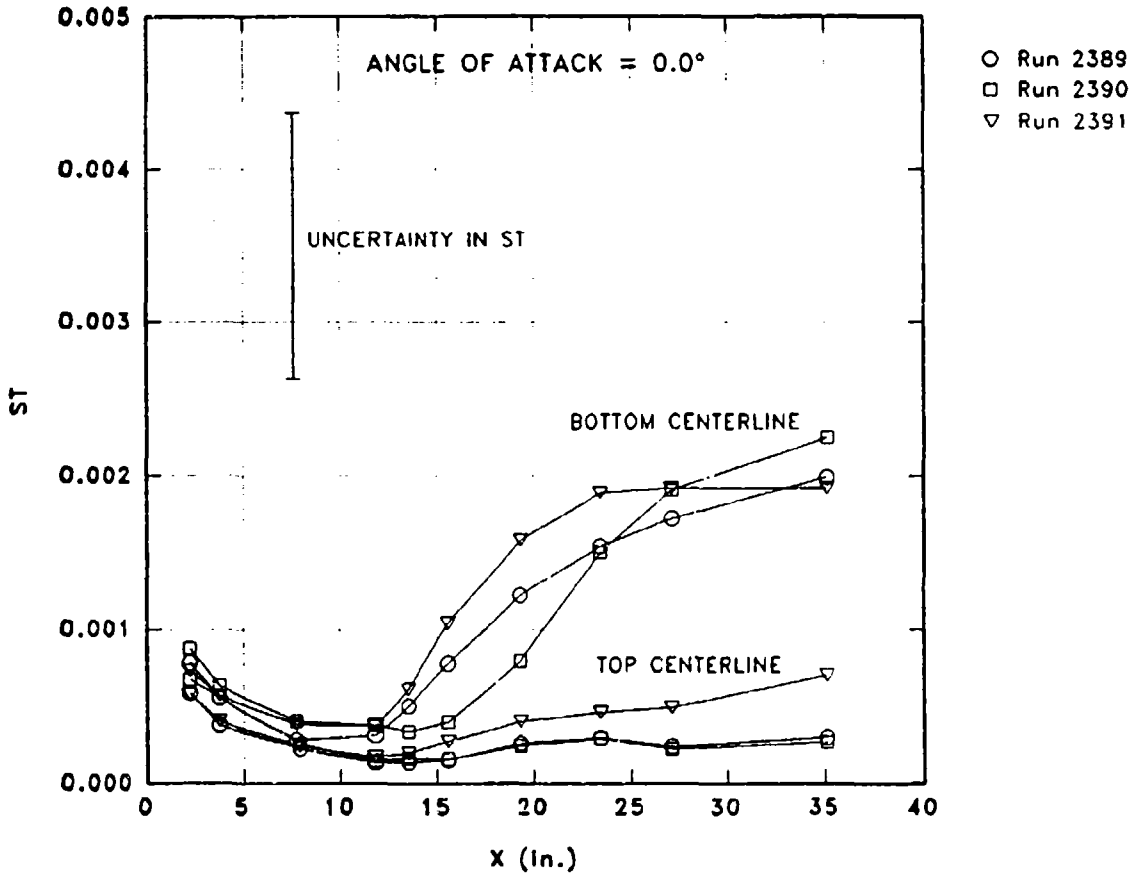

FIGURE 35. AXIAL VARIATIONS IN ST FOR ALPHA = 0.0°

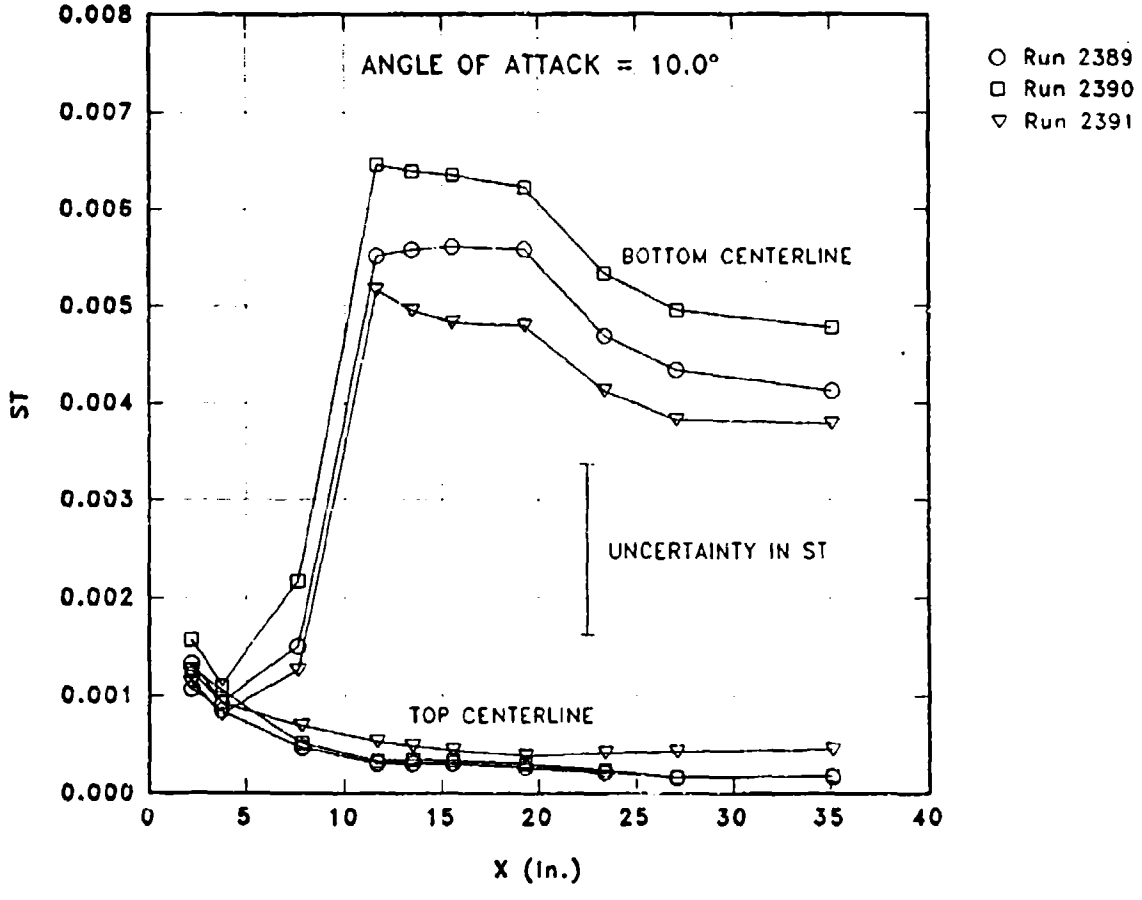

FIGURE 36. AXIAL VARIATIONS IN ST FOR ALPHA = 10.0°

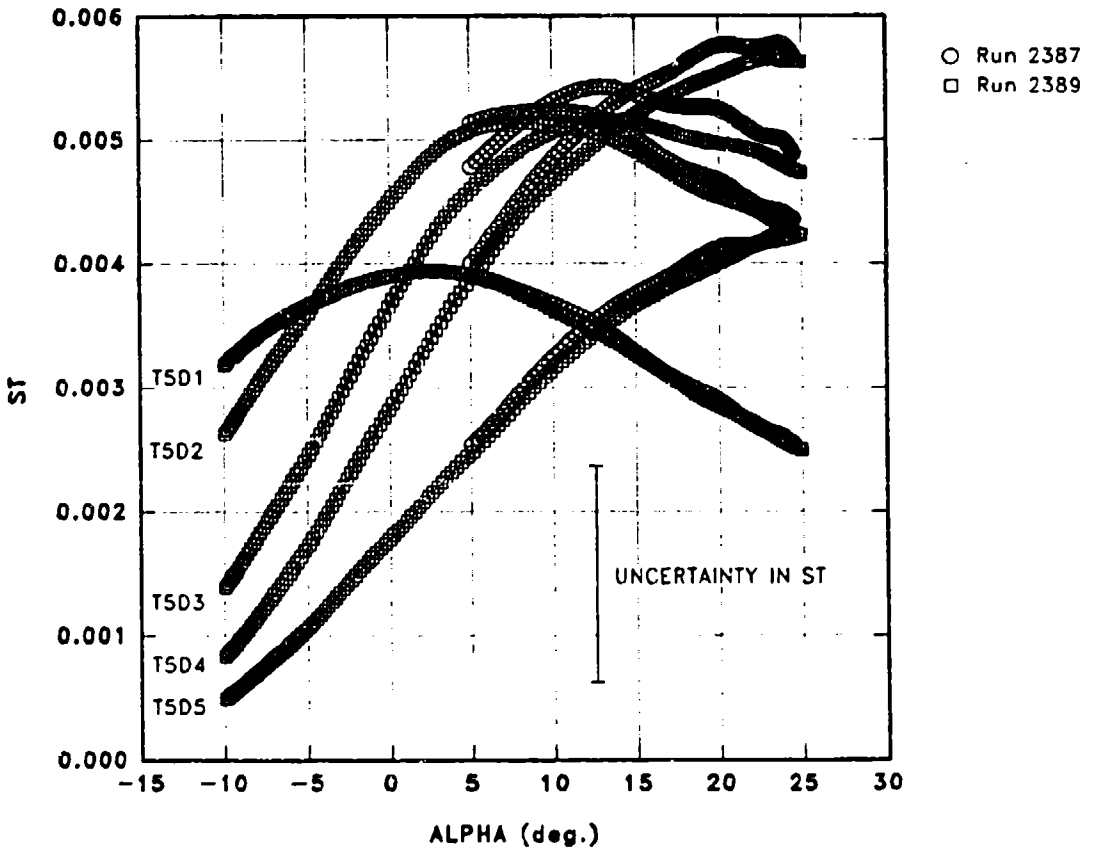

FIGURE 37. MACH-NUMBER EFFECTS ON LEADING-EDGE ST VS. ALPHA

TABLE 1. NOMINAL TEST CONDITIONS

MACH	9.7	10.4	13.9	16.7
P0 (psia)	1,300	14,000	9,400	21,000
T0 (°R)	1,835	1,850	3,050	2,880
REINF (1/ft)	2.0×10^6	20.0×10^6	2.0×10^6	3.2×10^6
QINF (psia)	2.4	23.0	3.2	3.4
UINF (ft/s)	4,650	4,900	6,450	6,400
PINF (psia)	0.037	0.320	0.024	0.018
TINF (°R)	92	90	88	60
Run time (s)	1.5	0.2	1.0	3.0

TABLE 2. SPECIFICATIONS AND ESTIMATED UNCERTAINTIES - TUNNEL INSTRUMENTATION

QTY units	Type	Range	B	S	dof	U_{ns}
Supply pressure, P0 psi	Viatran 304	10000	13.0	0.98	>30	13.1
	Viatran 121	20000	53.5	3.0	>30	53.8
	Viatran 214	50000	69.4	5.0	>30	69.7
Supply temperature, T0 °F	chromel vs alumel	~2000	18.2	0.015	>30	18.2
	W5RE vs W26RE	5000	14.0	0.032	>30	14.0
Test cell Pitot pressure, PT psi	Micro Switch 135PC15A1	15	0.014	0.007	>30	0.020
	Statham PA208TC	50	0.036	0.010	>30	0.041
Sector angle, THETAS deg	Houston Scientific 1150	-	0.017	0.017	>30	0.038

TABLE 3. SPECIFICATIONS AND ESTIMATED UNCERTAINTIES - MODEL INSTRUMENTATION

QTY units	Type	Range	B	S	dof	U_{ns}
Force balance 9HV6-3.						
Normal force, FN lbf	Able 1.5 inch Mk 34a	2000	6.48	A. 0.093 B. 0.051 C. 0.062	10	A. 6.48 B. 6.48 C. 6.48
Side force, FY lbf		500	2.05	A. 0.177 B. 0.290 C. 0.092	10	A. 2.09 B. 2.15 C. 2.06
Pitching moment, MY in-lbf		-	6.59	A. 6.590 B. 4.561 C. 0.211	10	A. 16.11 B. 12.12 C. 6.61
Yawing moment, MZ in-lbf		-	5.96	A. 0.288 B. 0.293 C. 1.340	10	A. 6.00 B. 6.00 C. 6.67
Rolling moment, MX in-lbf		800	1.13	A. 0.050 B. 0.053 C. 0.092	10	A. 1.14 B. 1.14 C. 1.15
Axial force, FA lbf		600	0.41	A. 0.275 B. 0.194 C. 0.155	10	A. 0.74 B. 0.60 C. 0.54
Pressure instrumentation.						
Base pressure, PB psia	Kulite XCW-062-5A	5	0.004	0.0004	>30	0.004
Surface pressure, P psia	Kulite XCW-062-5A	5	A,C. 0.018 B. 0.028	A,C. 0.006 B. 0.009	>30	A,C. 0.022 B. 0.033
	Kulite XCW-093-15A	15	A,C. 0.013 B. 0.013	A,C. 0.016 B. 0.009	>30	A,C. 0.035 B. 0.022
Heat transfer instrumentation.						
Surface temp. rise, °F	Medtherm TCS-E-10370	-	1.0	0.003	>30	1.0

A. Slow alpha sweep. B. Fast alpha sweep, Run 2394. C. Beta sweep, Run 2388.

TABLE 4. GAGE COORDINATE LOCATIONS AND NOMENCLATURE

Gauge Id.	X loc.	Y loc.	Z loc	Wall Thickness
TN	0.000	0.000	0.000	1.500
T1A	2.145	0.000	0.256	0.270
T1D	1.950	0.814	-0.550	0.310
T1G	2.145	0.000	-0.471	0.290
T2A	3.705	0.000	0.256	0.270
T2D1	4.095	1.671	-0.609	0.540
T2D2	3.900	1.598	-0.785	0.530
T2D3	3.705	1.421	-0.858	0.300
T2E	3.900	0.688	-0.836	0.230
T2G	3.705	0.000	-0.769	0.530
T3A	7.800	0.000	0.256	0.270
T3C	7.800	1.375	-0.300	0.340
T3D	7.800	2.407	-1.431	0.310
T3E	7.800	1.375	-1.438	0.800
T3G	7.605	0.000	-1.377	0.760
T4A	11.700	0.000	0.256	0.370
T4G	11.700	0.000	-2.030	-
T5A	13.455	0.000	0.256	0.370
T5B	13.650	1.194	-0.208	0.300
T5C	13.650	2.407	-0.890	0.280
T5D1	13.845	3.977	-2.012	0.360
T5D2	13.748	3.938	-2.094	0.360
T5D3	13.650	3.864	-2.162	0.380
T5D4	13.553	3.763	-2.203	0.460
T5D5	13.455	3.624	-2.209	0.250

TABLE 4. GAGE COORDINATE LOCATIONS AND NOMENCLATURE (CONTINUED)

Gauge Id.	X loc.	Y loc.	Z loc	Wall Thickness
T5E	13.650	2.407	-2.297	0.240
T5F	13.650	1.194	-2.355	-
T5G	13.455	0.000	-2.315	-
T6A	15.600	0.000	0.256	0.370
T6G	15.600	0.000	-2.664	-
T7A	19.305	0.000	0.256	0.370
T7B	19.500	1.706	-0.480	0.340
T7C	19.500	3.438	-1.528	0.310
T7D	19.500	4.818	-3.041	0.270
T7E	19.500	3.438	-3.106	0.310
T7F	19.500	1.706	-3.272	-
T7G	19.305	0.000	-3.272	-
T8A	23.400	0.000	0.256	0.370
T8G	23.400	0.000	-3.952	-
T9A	27.105	0.000	0.256	0.370
T9B	27.300	2.388	-0.879	0.260
T9C	27.300	4.814	-2.473	0.300
T9D	27.300	6.123	-4.197	0.240
T9E	27.300	4.184	-4.134	0.350
T9F	27.300	2.388	-4.488	-
T9G	27.105	0.000	-4.571	-
T10A	35.100	0.000	0.256	-
T10G	35.100	0.000	-5.919	-
P1A	1.755	0.000	0.256	-
P1G	1.755	0.000	-0.531	-

TABLE 4. GAGE COORDINATE LOCATIONS AND NOMENCLATURE (CONTINUED)

Gauge Id.	X loc.	Y loc.	Z loc	Wall Thickness
P2A	4.095	0.000	0.256	-
P2G	4.095	0.000	-0.829	-
P3C	7.800	-1.375	-0.300	-
P3G	7.995	0.000	-1.440	-
P5A	13.845	0.000	0.256	-
P5B	13.650	-1.194	-0.207	-
P5C	13.650	-2.407	-0.890	-
P5E	13.650	-2.407	-2.297	-
P5F	13.650	-1.194	-2.355	-
P5G	13.845	0.000	-2.378	-
P6D1	15.600	-4.330	-2.250	-
P6D2	15.795	-4.095	-2.526	-
P7A	19.695	0.000	0.256	-
P7C	19.500	-3.438	-1.528	-
P7E	19.500	-3.438	-3.106	-
P7G	19.695	0.000	-3.337	-
P9A	27.495	0.000	0.256	-
P9B	27.300	-2.388	-0.879	-
P9C	27.300	-4.814	-2.473	-
P9E	27.300	-4.814	-4.133	-
P9F	27.300	-2.388	-4.489	-
P9G	27.495	0.000	-4.636	-

TABLE 5. INOPERATIVE INSTRUMENTATION

Run	Inoperative Instrumentation
2387	P9C
2388	P9C, PB3, T0A
2389	P9C, PB3, PB8, T0A, P6D2 saturated for ALPHA>20
2390	PB8, T0B, T2A
2391	P7E
2393	P1G
2394	TN, T5D4, T9G
2395	T0B, TN, T5D4, T9G

TABLE 6. BASE PRESSURE TAP AREA ASSIGNMENTS

Base pressure tap	Area (in^2)
PB1	6.9
PB2	7.2
PB3	10.5
PB4	8.0
PB5	6.3
PB6	8.0
PB7	10.5
PB8	7.2
Total Base area	64.6

TABLE 7. ESTIMATED UNCERTAINTIES - CALCULATED PARAMETERS

Parameter units	Nominal value	B	P	U_{rss}	Comment
MACH	9.65e+00	2.26e-02	7.12e-03	2.37e-02	All runs
PINF psia	3.17e-01	9.62e-04	2.15e-04	9.86e-04	REINF = 20e+06 ft^{-1}
	3.82e-02	2.38e-04	1.68e-04	2.91e-04	REINF = 2,3e+06 ft^{-1}
QINF psia	2.44e+01	1.95e-02	1.08e-02	2.23e-02	REINF = 20e+06 ft^{-1}
	3.18e+00	7.60e-03	7.59e-03	1.08e-02	REINF = 2,3e+06 ft^{-1}
REINF ft^{-1}	1.94e+07	3.30e+05	6.24e+03	3.30e+05	REINF = 20e+06 ft^{-1}
	1.91e+06	3.26e+04	3.73e+03	3.29e+04	REINF = 2,3e+06 ft^{-1}
RHOINF lbm/ft^3	9.19e-03	9.44e-05	4.18e-06	9.45e-05	REINF = 20e+06 ft^{-1}
	1.02e-03	1.14e-05	3.17e-06	1.18e-05	REINF = 2,3e+06 ft^{-1}
TINF °R	9.75e+01	1.19e+00	1.36e-01	1.20e+00	Mach 10
	8.52e+01	5.54e-01	8.54e-02	5.61e-01	Mach 14/16.5
UINF ft/s	4.75e+03	2.54e+01	1.95e-01	2.54e+01	Mach 10
	6.46e+03	1.63e+01	1.64e-01	1.63e+01	Mach 14/16.5
VIP $ft^{1/2}$	6.99e-03	5.63e-05	1.11e-05	5.74e-05	REINF = 2,3e+06 ft^{-1}
	2.38e-03	1.80e-05	5.55e-07	1.80e-05	REINF = 20e+06 ft^{-1}
CP	8.46e-01	6.64e-03	2.93e-03	7.26e-03	REINF = 2,3e+06 ft^{-1}
	1.44e-01	7.30e-04	1.50e-04	7.46e-04	REINF = 20e+06 ft^{-1}
P/P01	1.67e-03	2.24e-05	3.64e-06	2.27e-05	P0 = 1300 psia
	2.41e-04	2.65e-06	4.03e-07	2.68e-06	P0 = 9400, 14000, 21000 psia
P/PINF	1.20e+02	9.55e-01	4.09e-01	1.04e+00	REINF = 2,3e+06 ft^{-1}
	1.21e+01	6.57e-02	1.30e-02	6.70e-02	REINF = 20e+06 ft^{-1}

TABLE 7. ESTIMATED UNCERTAINTIES - CALCULATED PARAMETERS (CONTINUED)

Parameter units	Nominal value	B	P	U_{rss}	Comment
P/PT	4.66e-01	3.59e-03	1.58e-03	3.93e-03	REINF = 2,3e+06 ft^{-1}
	8.52e-02	3.95e-04	8.06e-05	4.03e-04	REINF = 20e+06 ft^{-1}
ST	5.00e-03	-	8.70e-04	8.70e-04	All runs
AFC	1.21e-01	6.13e-04	6.70e-04	9.08e-04	REINF = 2,3e+06 ft^{-1}
	2.27e-02	7.46e-05	6.23e-05	9.72e-05	REINF = 20e+06 ft^{-1}
ALPHA deg	9.91e+00	8.92e-02	2.90e-02	9.37e-02	All runs
BETA deg	-1.04e+00	4.16e-02	2.38e-02	4.79e-02	All runs
BETAP deg	-1.05e+00	4.20e-02	2.42e-02	4.85e-02	All runs
CAFC	1.20e-01	6.53e-04	6.73e-04	9.37e-04	REINF = 2,3e+06 ft^{-1}
	2.07e-02	8.01e-05	6.27e-05	1.02e-04	REINF = 20e+06 ft^{-1}
CDS	4.02e-01	2.65e-03	1.11e-03	2.87e-03	REINF = 2,3e+06 ft^{-1}
	2.52e-02	1.11e-04	5.56e-05	1.25e-04	REINF = 20e+06 ft^{-1}
CLS	6.49e-02	7.09e-03	3.03e-04	7.09e-03	REINF = 2,3e+06 ft^{-1}
	9.73e-02	6.99e-04	4.47e-05	7.00e-04	REINF = 20e+06 ft^{-1}
CPB	-1.12e-02	1.64e-03	3.30e-04	1.68e-03	REINF = 2,3e+06 ft^{-1}
	-1.14e-02	1.65e-04	3.25e-05	1.69e-04	REINF = 20e+06 ft^{-1}
NFC	6.49e-02	7.09e-03	3.03e-04	7.09e-03	REINF = 2,3e+06 ft^{-1}
	9.80e-02	6.99e-04	4.53e-05	7.01e-04	REINF = 20e+06 ft^{-1}

TABLE 7. ESTIMATED UNCERTAINTIES - CALCULATED PARAMETERS (CONTINUED)

Parameter units	Nominal value	B	P	U_{rss}	Comment
PMC	-4.32e-02	4.60e-03	4.61e-04	4.62e-03	REINF = 2,3e+06 ft^{-1}
	-6.36e-02	4.54e-04	4.05e-05	4.56e-04	REINF = 20e+06 ft^{-1}
PMCS	-4.32e-02	4.60e-03	4.61e-04	4.62e-03	REINF = 2,3e+06 ft^{-1}
	-6.36e-02	4.54e-04	4.05e-05	4.56e-04	REINF = 20e+06 ft^{-1}
RMC	7.89e-04	1.36e-04	2.51e-05	1.38e-04	REINF = 2,3e+06 ft^{-1}
	-7.96e-05	1.80e-05	4.41e-06	1.85e-05	REINF = 20e+06 ft^{-1}
RMCS	8.92e-04	6.10e-04	1.45e-04	6.27e-04	REINF = 2,3e+06 ft^{-1}
	-1.10e-04	2.06e-05	5.82e-06	2.14e-05	REINF = 20e+06 ft^{-1}
YFC	2.19e-03	2.24e-03	4.33e-04	2.28e-03	REINF = 2,3e+06 ft^{-1}
	1.93e-03	2.26e-04	8.06e-05	2.40e-04	REINF = 20e+06 ft^{-1}
YFCS	2.19e-03	2.24e-03	4.33e-04	2.28e-03	REINF = 2,3e+06 ft^{-1}
	1.93e-03	2.26e-04	8.06e-05	2.40e-04	REINF = 20e+06 ft^{-1}
YMC	-1.37e-03	1.52e-03	2.92e-04	1.54e-03	REINF = 2,3e+06 ft^{-1}
	-1.16e-03	1.52e-04	5.35e-05	1.61e-04	REINF = 20e+06 ft^{-1}
YMCS	-1.37e-03	1.52e-03	2.92e-04	1.55e-03	REINF = 2,3e+06 ft^{-1}
	-1.16e-03	1.52e-04	5.34e-05	1.61e-04	REINF = 20e+06 ft^{-1}
XCPP	-6.53e-01	5.40e-04	2.32e-03	2.38e-03	All runs
XCPY	-6.26e-01	8.88e-02	1.20e-02	8.96e-02	All runs

TABLE 8. ESTIMATED UNCERTAINTIES - CALCULATED LIFT-TO-DRAG RATIO

Nominal L/D	ALPHA deg	B	P	U_{rss}
-3.44	-10.0	1.74e-01	1.31e-01	2.18e-01
2.86	-5.0	7.25e-01	4.70e-02	7.27e-01
3.58	0.0	3.21e-01	1.08e-01	3.38e-01
3.23	5.00	9.86e-02	4.13e-02	1.07e-01
2.58	10.0	3.51e-02	1.58e-02	3.85e-02
2.08	15.0	1.61e-02	7.38e-03	1.77e-02
1.71	20.0	8.79e-03	4.03e-03	9.67e-03
1.43	25.0	5.42e-03	2.44e-03	5.94e-03

TABLE 9. RUN MATRIX

Run	MACH	REINF ft^{-1}	Sweep	Comment
2387	14	2.0×10^6	ALPHA +5° to +25°	Pitch stability at design condition.
2388	14	2.0×10^6	BETA -5° to +5°	Yaw stability at design condition.
2389	14	2.0×10^6	ALPHA -10° to +25°	Repeat of 2387.
2390	16.5	3.2×10^6	ALPHA -10° to +25°	Off-design Mach number effects.
2391	10	2.0×10^6	ALPHA -10° to +25°	Off-design Mach number effects.
2393	10	2.0×10^6	ALPHA 10° fixed	Temperature-sensitive paint test.
2394	10	20.0×10^6	ALPHA -10° to +4°	Reynolds number effects. Gritted nose for turbulent boundary layer.
2395	10	2.0×10^6	ALPHA +10° to -25°	Temperature-sensitive paint test. Model inverted for flow angularity check.

REFERENCES

1. Ragsdale, W., and Boyd, C., *Hypervelocity Wind Tunnel 9 Facility Handbook*, Third Edition, NAVSWC TR 91-616, 26 Jul 1993, NSWCDD, Silver Spring, MD.

2. Burnett, D., and Lewis, M., "A Re-Evaluation of the Waverider Design Process," AIAA Paper 93-0404, Jan 1993.

3. Berry, C., et al., "Experiences in Fabrication of a Waverider Model for Wind Tunnel Testing," AIAA Paper 93-0510, Jan 1993.

4. Hedlund, E., et al., *Heat Transfer Testing in the NSWC Hypervelocity Wind Tunnel Utilizing Co-axial Surface Thermocouples*, NSWC MP 80-151, Mar 1980, NSWC, Silver Spring, MD.

5. NSWC K24 Memo, Subj: COAX Heat Gage Data Reduction, Silver Spring, MD, 21 Jul 1987.

6. Sullivan, John P., et al., "Remote Temperature and Heat Transfer Mapping for Waverider Model at Mach 10 Using Fluorescent Paint," AIAA Paper 94-2484, Jun 1994.

7. Boyd, C., Ragsdale, W., and Knott, J., *Wind Tunnel Model Force Measurements at the Naval Surface Warfare Center*, NAVSWC TR 91-372, Sep 1991, NAVSWC, Silver Spring, MD.

8. Wright, John, *A Compilation of Aerodynamic Nomenclature and Axes Systems*, NOL Report No. 1241, Aug 1962.

9. *Measurement Uncertainty*, ANSI/ASME PTC 19.1-1985 Part 1, 1986.

10. NSWCDD/WODET K24 Memo, Subj: Measurement Uncertainty for Tunnel 9, Silver Spring, MD, 27 Aug 1993.

11. Coleman, H. W., and Steele, W. G., *Experimentation and Uncertainty Analysis for Engineers*, John Wiley & Sons, Inc., New York, NY, 1989.

12. SECNAVINST 3960.6 of 12 Oct 1990, Subj: Department of the Navy Policy and Responsibility for Test, Measurement, Monitoring, Diagnostic Equipment and Systems, and Metrology and Calibration (METCAL), Washington, DC.

NOMENCLATURE

ABASE	Base area, 64.6 in^2
AFB	Air Force Base
AFC	Axial-force coefficient, body axes, axial force/(QINF*AREF)
ALPHA	Angle of attack, deg
AREF	Reference area, 375.3 in^2
B	Bias error at 95% confidence level
BETA	Sideslip angle, stability axes, deg
BETAP	Sideslip angle, body axes, deg
BMO	Ballistic Missile Organization
Cp	Specific heat of nitrogen at constant pressure
CAC	Corrected axial-force coefficient, body axes, AFC + CPB*(ABASE/AREF)
CDS	Drag coefficient, stability axes
CLS	Lift coefficient, stability axes
CNC	Computer numerically controlled
CP	Pressure coefficient, (pressure - PINF)/QINF
CPB	Base pressure coefficient, (PB - PINF)/QINF
DARE	Data Acquisition and Recording Equipment
dof	Number of degrees of freedom associated with a standard deviation calculation

L	Model reference length, 39.000 in
L/D	Lift-to-drag ratio based on AFC, stability axes
MACH	Free-stream Mach number
MAXWARP	University of Maryland Axisymmetric Waverider Program
METCAL	Metrology and Calibration
MRC	Moment reference center, model coordinates (X,Y,Z)=(0,0,0)
NFC	Normal-force coefficient, body axes, normal force/(QINF*AREF)
NSWC	Naval Surface Warfare Center
P	Precision error at 95% confidence level, $t_{95}S$
PB	Integrated base pressure, psia
PB1-8	Base pressures 1-8, psia
PINF	Free-stream pressure, psia
PMC	Pitching-moment coefficient, body axes, pitching moment/(QINF*AREF*L)
PMCS	Pitching-moment coefficient, stability axes
P0	Tunnel supply pressure, psia
P01	Tunnel equivalent-perfect-gas supply pressure, psia
PTN	North test cell Pitot pressure, psia
PTS	South test cell Pitot pressure, psia
QINF	Free-stream dynamic pressure, psia
QDOT	Heat transfer rate, BTU/(ft^2*sec)

REINF/L	Free-stream Reynolds number, ft^{-1}
RHOINF	Free-stream static density, lbm/ft^3
RMC	Rolling-moment coefficient, body axes, rolling moment/(QINF*AREF*L)
RMCS	Rolling-moment coefficient, stability axes
S	Sample Standard deviation
ST	Stanton number, QDOT / {Cp*RHOINF*UINF[T01-(T+70°F)]}
t_{95}	95th percentile point for the two-tailed Student's "t" distribution (95-percent confidence interval), which for sample sizes greater than 30 is considered equal to 2.
T	Measured surface temperature rise, °F
THETAS	Pitch angle of model support system, deg
TINF	Free-stream static temperature, °R
T0	Tunnel supply temperature, °F
T0A, T0B	Measured tunnel supply temperatures in settling chamber, °F
T0C	Measured tunnel supply temperature upstream of particle separator, °F
T01	Tunnel equivalent-perfect-gas supply temperature, °F
U_{rss}	Uncertainty $[B^2 + P^2]^{1/2}$
UINF	Free-stream velocity, ft/sec
USAF	United States Air Force
X	Model station aft of nose, in

XCPP	Pitch center of pressure, fraction of model length aft of nose, MRC/L - PMC/NFC
XCPY	Yaw center of pressure, fraction of model length aft of nose, MRC/L - YMC/YFC
Y	Butt line location from model centerline, in
YFC	Yaw-force coefficient, body axes, yaw force/(QINF*AREF)
YFCS	Yaw-force coefficient, stability axes
YMC	Yawing-moment coefficient, body axes, yawing moment/(QINF*AREF*L)
YMCS	Yawing-moment coefficient, stability axes
Z	Model vertical location, in

DISTRIBUTION

	Copies
DOD ACTIVITIES (CONUS)	
DEFENSE TECHNICAL INFORMATION CENTER CAMERON STATION ALEXANDRIA VA 22304-6145	12
ATTN CODE E29L COASTAL SYSTEMS STATION DAHLGREN DIVISION NAVAL SURFACE WARFARE CENTER 6703 WEST HIGHWAY 98 PANAMA CITY FL 32407-7001	1
ATTN CAPT M STONE USAF BALLISTIC MISSILE ORGANIZATION PHILLIPS LABS/VT-B 3550 ABERDEEN AVENUE KIRTLAND AFB NM 87117-5776	5
ATTN DR T HOLTZ PL/VT-B 3550 ABERDEEN AVENUE KIRTLAND AFB NM 87117-5776	2
ATTN CODE SS (JAMES E RANDOLPH) NASA HEADQUARTERS SPACE PHYSICS DIVISION WASHINGTON DC 20546	1
ATTN DR JOHN ANDERSON NASA HEADQUARTERS WASHINGTON DC 20546	1
NON-DOD ACTIVITIES	
ATTN DAVID BURNETT MCDONNELL DOUGLAS AEROSPACE 5301 BOLSA AVENUE HUNTINGTON BEACH CA 92647	10
ATTN DR JOHN ANDERSON JR DR MARK LEWIS NASA CENTER FOR HYPERSONIC EDUCATION AND RESEARCH DEPT OF AEROSPACE ENGINEERING UNIVERSITY OF MARYLAND AT COLLEGE PARK 3172 ENGINEERING CLASSROOM BLDG COLLEGE PARK MD 20742-3015	4 4
ATTN DR JOHN P SULLIVAN SCHOOL OF AERONAUTICS AND ASTRONAUTICS PURDUE UNIVERSITY 1282 GRISSOM HALL WEST LAFAYETTE IN 47907-5117	2
ATTN PROF KARL BERGEY PROF MAURICE RASSMUSSEN PROF GEORGE EMANUEL UNIVERSITY OF OKLAHOMA DEPARTMENT OF AEROSPACE AND MECHANICAL ENGINEERING NORMAN OK 73019	1 1 1
ATTN GIFT AND EXCHANGE DIV LIBRARY OF CONGRESS WASHINGTON DC 20540	4
CENTER FOR NAVAL ANALYSES 4401 FORD AVENUE ALEXANDRIA VA 22302-0268	1
INTERNAL	
E231	2
E232	3
K24	100

REPORT DOCUMENTATION PAGE

Form Approved
OMB No. 0704-0188

1. AGENCY USE ONLY (Leave blank)	2. REPORT DATE	3. REPORT TYPE AND DATES COVERED
	5 May 1994	

4. TITLE AND SUBTITLE Design Validation Tests on a Realistic Hypersonic Waverider at Mach 10, 14, and 16.5 in the Naval Surface Warfare Center Hypervelocity Wind Tunnel No. 9

5. FUNDING NUMBERS

6. AUTHOR(S)

Mark E. Kammeyer and Michael J. Gillum

7. PERFORMING ORGANIZATION NAME(S) AND ADDRESS(ES)

Naval Surface Warfare Center (Code K24)
10901 New Hampshire Avenue
Silver Spring, MD 20903-5640

8. PERFORMING ORGANIZATION REPORT NUMBER

NSWCDD/TR-93/198

9. SPONSORING/MONITORING AGENCY NAME(S) AND ADDRESS(ES)

10. SPONSORING/MONITORING AGENCY REPORT NUMBER

11. SUPPLEMENTARY NOTES

12a. DISTRIBUTION/AVAILABILITY STATEMENT

Approved for public release; distribution is unlimited.

12b. DISTRIBUTION CODE

13. ABSTRACT *(Maximum 200 words)*

A realistic hypersonic waverider was tested in the Navy's Hypervelocity Wind Tunnel No. 9 in late Spring of 1993. Sponsored by the McDonnell Douglas Space Systems Company, Huntington Beach, and the United States Air Force Ballistic Missile Organization, Norton Air Force Base, tests at Mach numbers of 10, 14, and 16.5 were conducted to measure static stability and drag, to determine the distributions of surface pressure and heat transfer, and to obtain flow-visualization data.

The two principal objectives of this test program were to validate the methodology for designing performance-optimized hypersonic waveriders and to obtain data on a complex hypersonic configuration for validation of computational fluid dynamic codes. The waverider design included realistically blunted leading edges and was optimized on an arbitrary figure of merit to include fluid viscosity and internal volume. The design condition of Mach 14 and Reynolds number based on length of 6.5 million was chosen based on the facility capabilities.

All data appeared to be independent of Mach number and virtually insensitive to changes in Reynolds number; moreover, all data displayed excellent repeatability. The lift-to-drag ratio of this waverider with realistic leading-edge radii was found to be relatively high.

14. SUBJECT TERMS	15. NUMBER OF PAGES
Waverider CFD Leading Edges	83
	16. PRICE CODE

17. SECURITY CLASSIFICATION OF REPORT	18. SECURITY CLASSIFICATION OF THIS PAGE	19. SECURITY CLASSIFICATION OF ABSTRACT	20. LIMITATION OF ABSTRACT
UNCLASSIFIED	UNCLASSIFIED	UNCLASSIFIED	SAR

GENERAL INSTRUCTIONS FOR COMPLETING SF 298

The Report Documentation Page (RDP) is used in announcing and cataloging reports. It is important that this information be consistent with the rest of the report, particularly the cover and its title page. Instructions for filling in each block of the form follow. It is important to ***stay within the lines*** to meet ***optical scanning requirements.***

Block 1. Agency Use Only *(Leave blank)*.

Block 2. Report Date. Full publication date including day, month, and year, if available (e.g. 1 Jan 88). Must cite at least the year.

Block 3. Type of Report and Dates Covered. State whether report is interim, final, etc. If applicable, enter inclusive report dates (e.g. 10 Jun 87 - 30 Jun 88).

Block 4. Title and Subtitle. A title is taken from the part of the report that provides the most meaningful and complete information. When a report is prepared in more than one volume, repeat the primary title, add volume number, and include subtitle for the specific volume. On classified documents enter the title classification in parentheses.

Block 5. Funding Numbers. To include contract and grant numbers; may include program element number(s), project number(s), task number(s), and work unit number(s). Use the following labels:

C	- Contract	**PR**	- Project
G	- Grant	**TA**	- Task
PE	- Program Element	**WU**	- Work Unit Accession No.

BLOCK 6. Author(s). Name(s) of person(s) responsible for writing the report, performing the research, or credited with the content of the report. If editor or compiler, this should follow the name(s).

Block 7. Performing Organization Name(s) and Address(es). Self-explanatory.

Block 8. Performing Organization Report Number. Enter the unique alphanumeric report number(s) assigned by the organization performing the report.

Block 9. Sponsoring/Monitoring Agency Name(s) and Address(es). Self-explanatory.

Block 10. Sponsoring/Monitoring Agency Report Number. *(If Known)*

Block 11. Supplementary Notes. Enter information not included elsewhere such as: Prepared in cooperation with...; Trans. of...; To be published in.... When a report is revised, include a statement whether the new report supersedes or supplements the older report.

Block 12a. Distribution/Availability Statement. Denotes public availability or limitations. Cite any availability to the public. Enter additional limitations or special markings in all capitals (e.g. NOFORN, REL, ITAR).

DOD	- See DoDD 5230.24, "Distribution Statements on Technical Documents."
DOE	- See authorities.
NASA	- See Handbook NHB 2200.2
NTIS	- Leave blank.

Block 12b. Distribution Code.

DOD	- Leave blank.
DOE	- Enter DOE distribution categories from the Standard Distribution for Unclassified Scientific and Technical Reports.
NASA	- Leave blank.
NTIS	- Leave blank.

Block 13. Abstract. Include a brief ***(Maximum 200 words)*** factual summary of the most significant information contained in the report.

Block 14. Subject Terms. Keywords or phrases identifying major subjects in the report.

Block 15. Number of Pages. Enter the total number of pages.

Block 16. Price Code. Enter appropriate price code ***(NTIS only)***

Blocks 17.-19. Security Classifications. Self-explanatory. Enter U.S. Security Classification in accordance with U.S. Security Regulations (i.e., UNCLASSIFIED). If form contains classified information, stamp classification on the top and bottom of the page.

Block 20. Limitation of Abstract. This block must be completed to assign a limitation to the abstract. Enter either UL (unlimited) or SAR (same as report). An entry in this block is necessary if the abstract is to be limited. If blank, the abstract is assumed to be unlimited.

DEPARTMENT OF THE NAVY
NAVAL SURFACE WARFARE CENTER
DAHLGREN, VIRGINIA 22448-5000

WHITE OAK
10901 NEW HAMPSHIRE AVE.
SILVER SPRING, MD 20903-5000
(301) 394-1669

DAHLGREN, VA 22448-5000
(703) 663-

ERRATA AD-A279 698

IN RELY REFER TO:
K24:MEK
Change 1

9 Nov 1994

To all holders of NSWCDD/TR-93/198
Title: Design Validation Tests on a Realistic Hypersonic Waverider at Mach 10, 14, and 16.5 in the Naval Surface Warfare Center Hypervelocity Wind Tunnel No. 9

11 page(s)

This publication is changed as follows:

Remove the following pages and replace with new pages supplied:

47 through 54
63/64

Make the following pen-and-ink change:

Page 65, Table 8, third row, first column, change "2.86" to "0.73"

Dispose of the removed pages in accordance with applicable security regulations.

Insert this change sheet directly behind the front cover in your copy.
Write on the cover "Change 1 inserted"

Approved by:

R. L. SCHMIDT

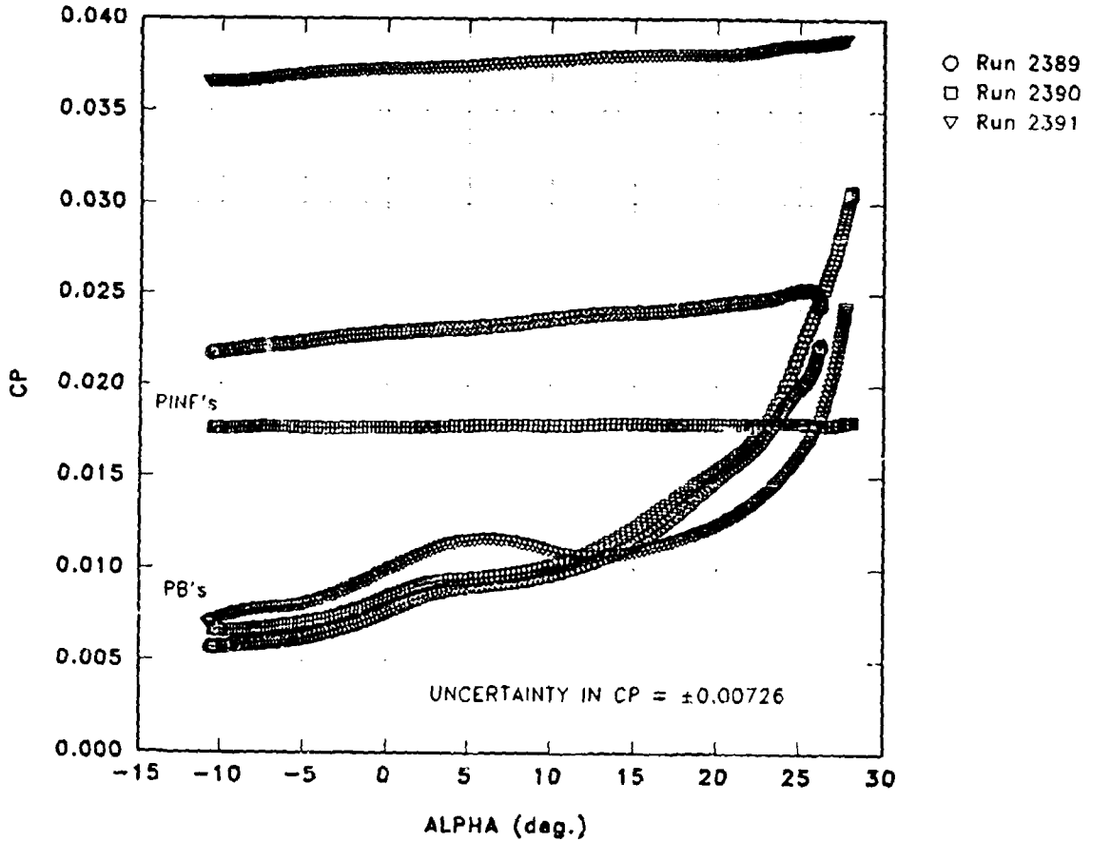

FIGURE 31. MACH-NUMBER EFFECTS ON BASE AND FREESTREAM CP'S

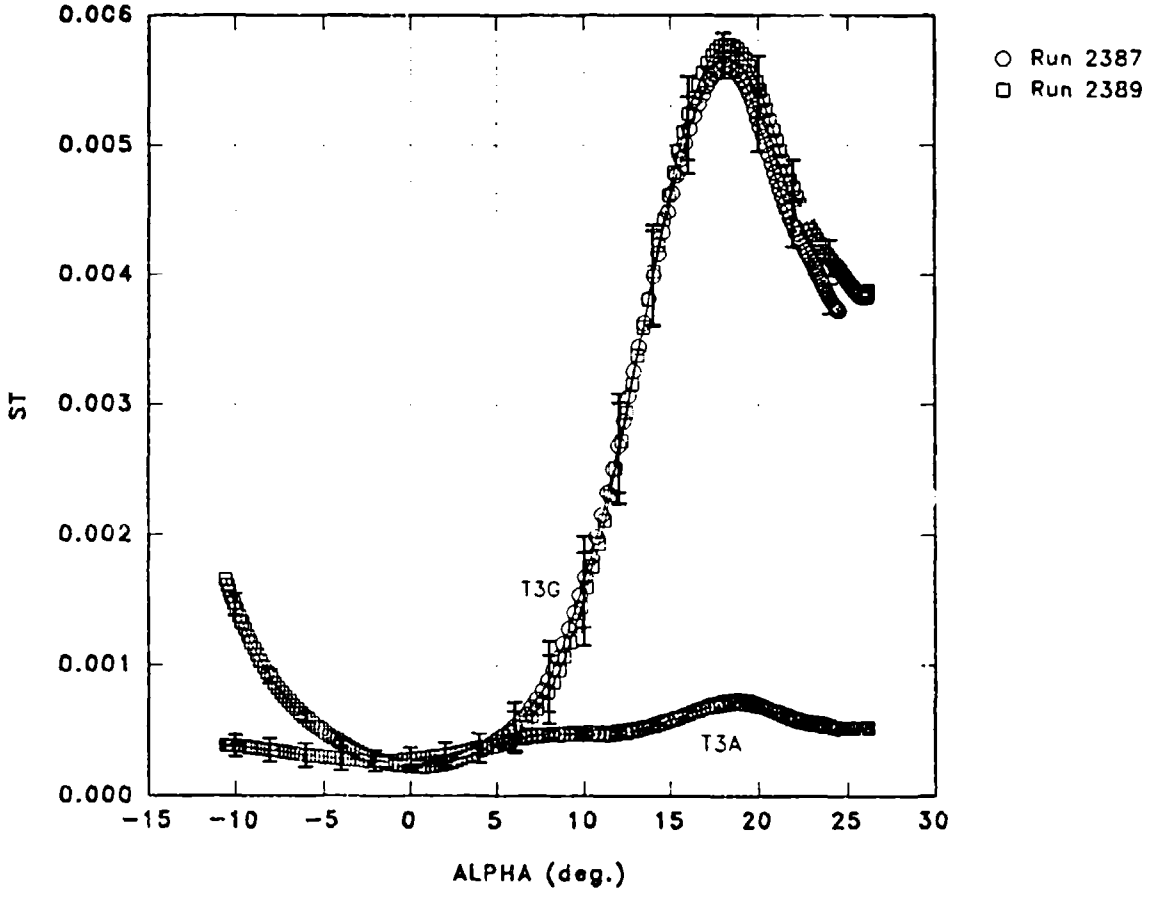

FIGURE 32. STANTON NUMBER VS. ALPHA FOR DESIGN CONDITION

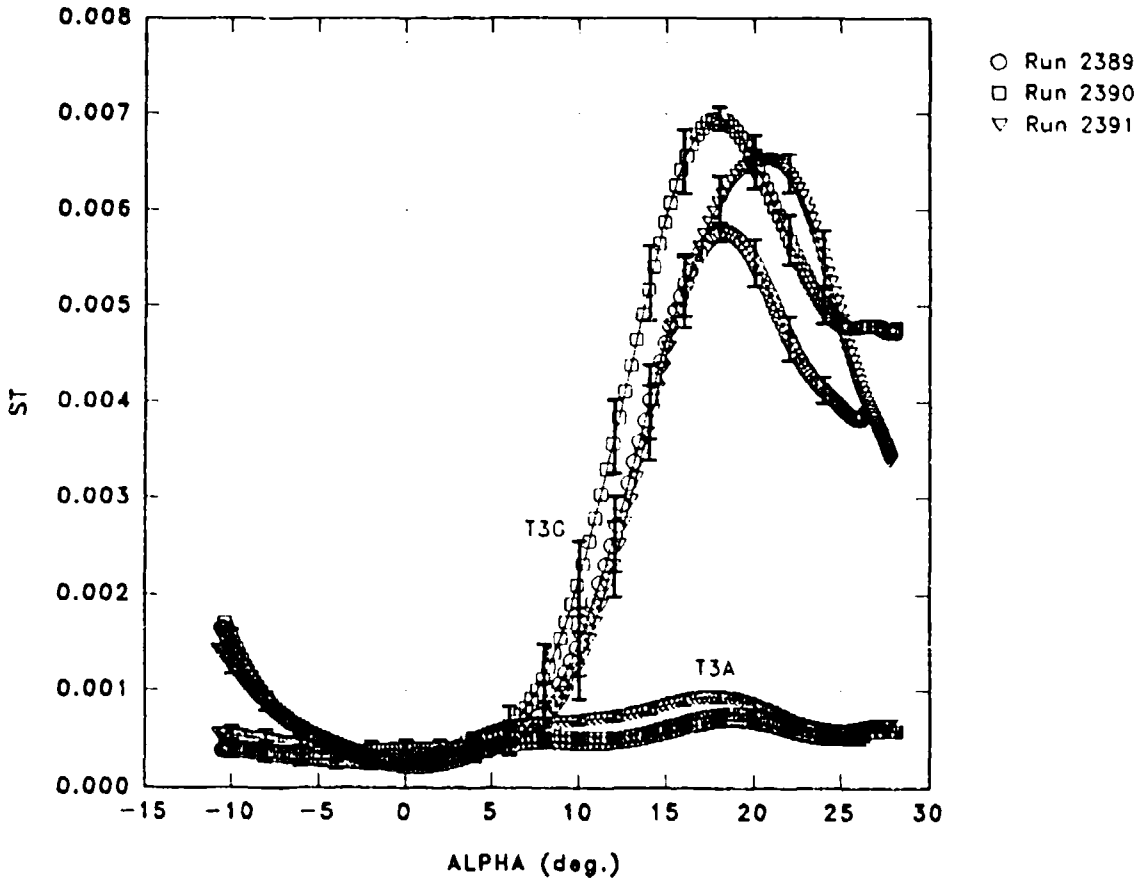

FIGURE 33. MACH-NUMBER EFFECTS ON ST VS. ALPHA

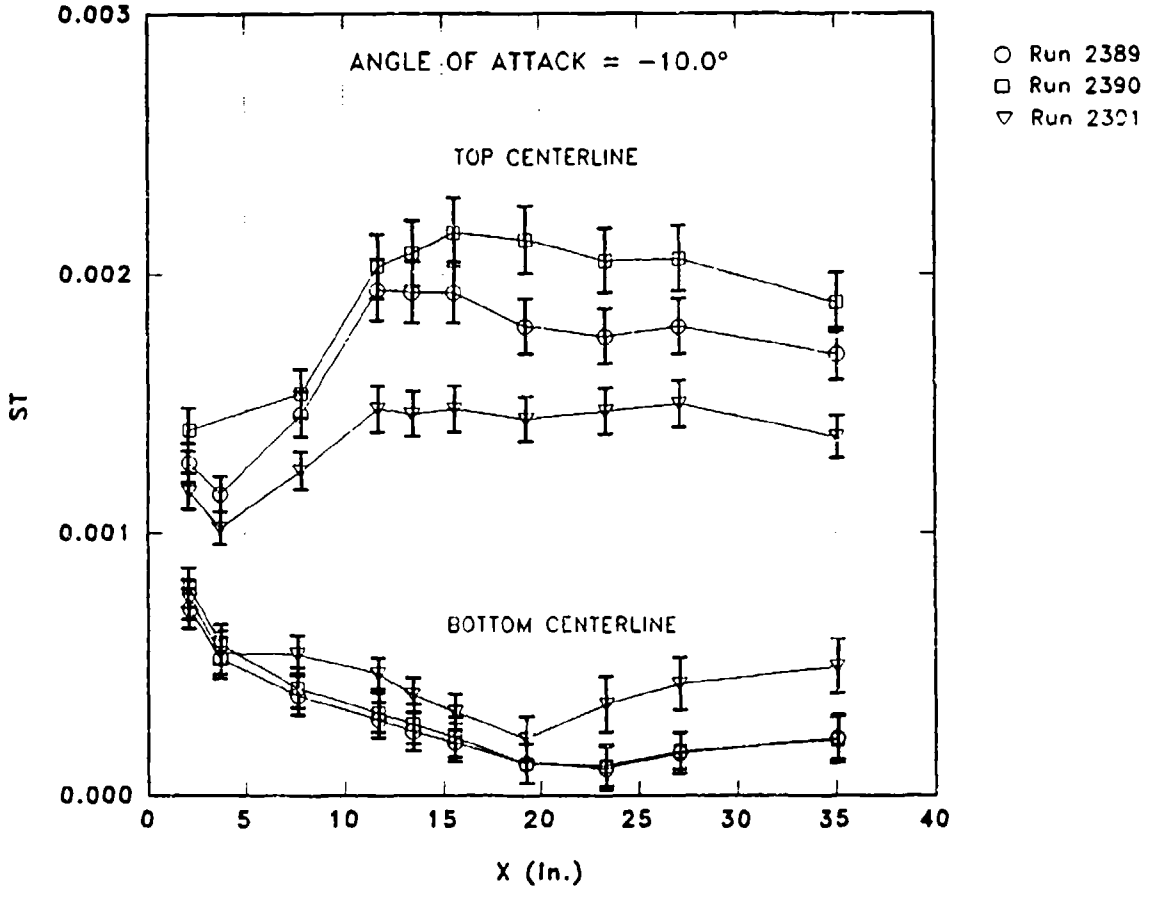

FIGURE 34. AXIAL VARIATIONS IN ST FOR ALPHA = -10.0°

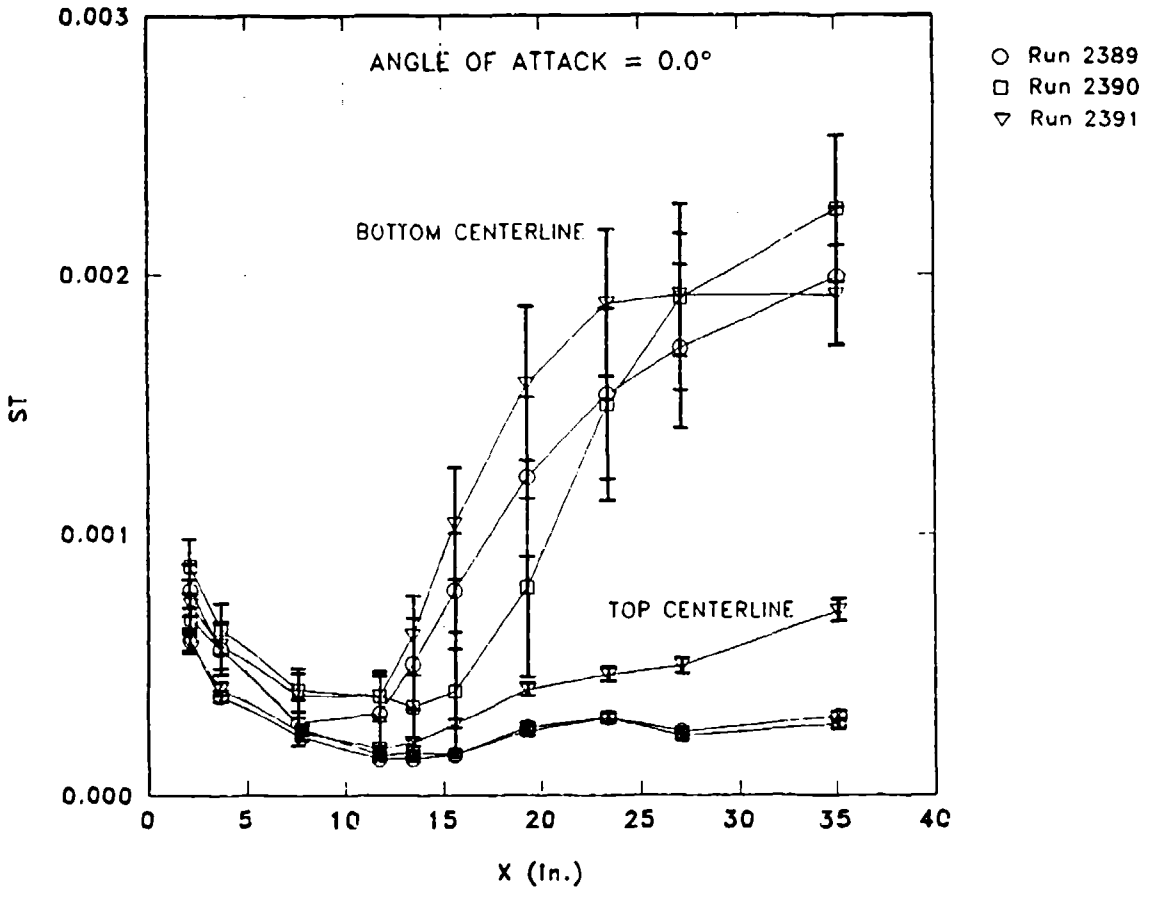

FIGURE 35. AXIAL VARIATIONS IN ST FOR ALPHA = 0.0°

Change 1

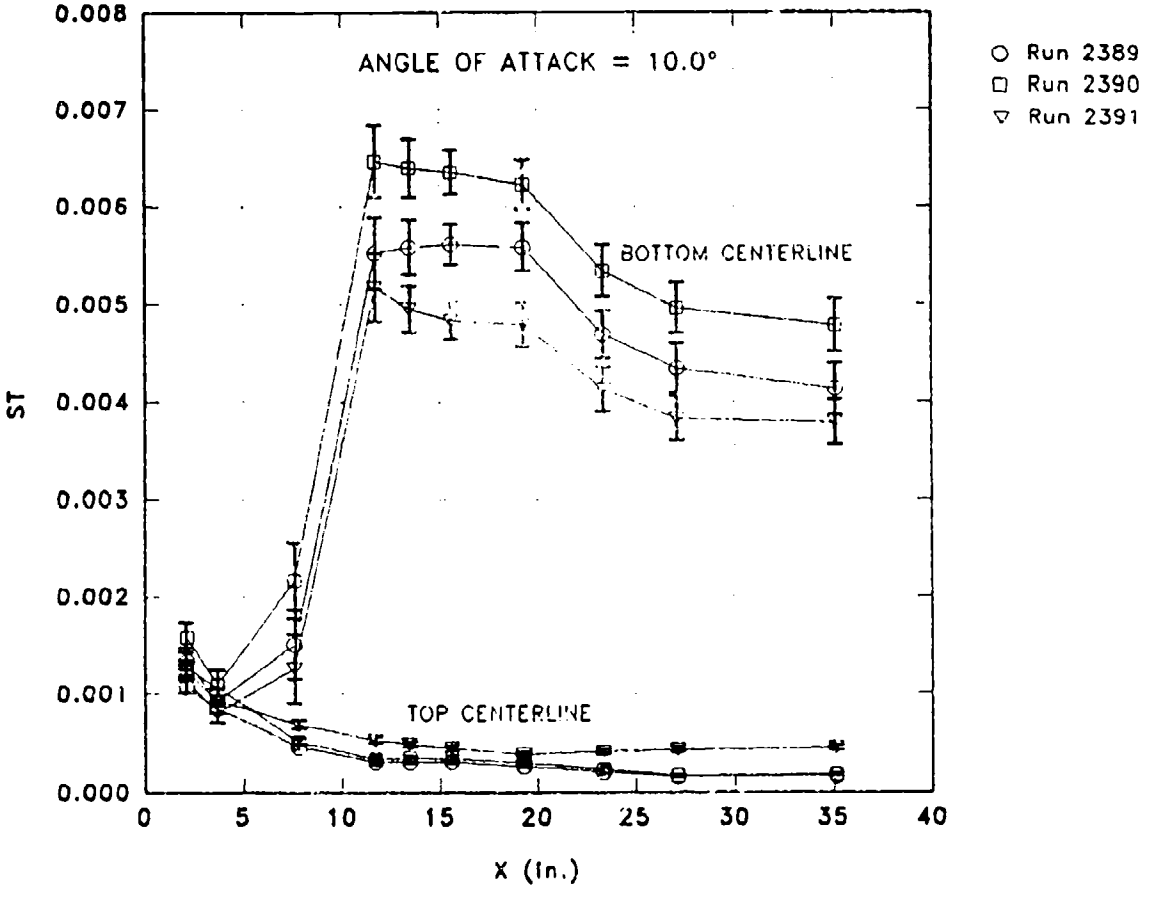

FIGURE 36. AXIAL VARIATIONS IN ST FOR ALPHA = 10.0°

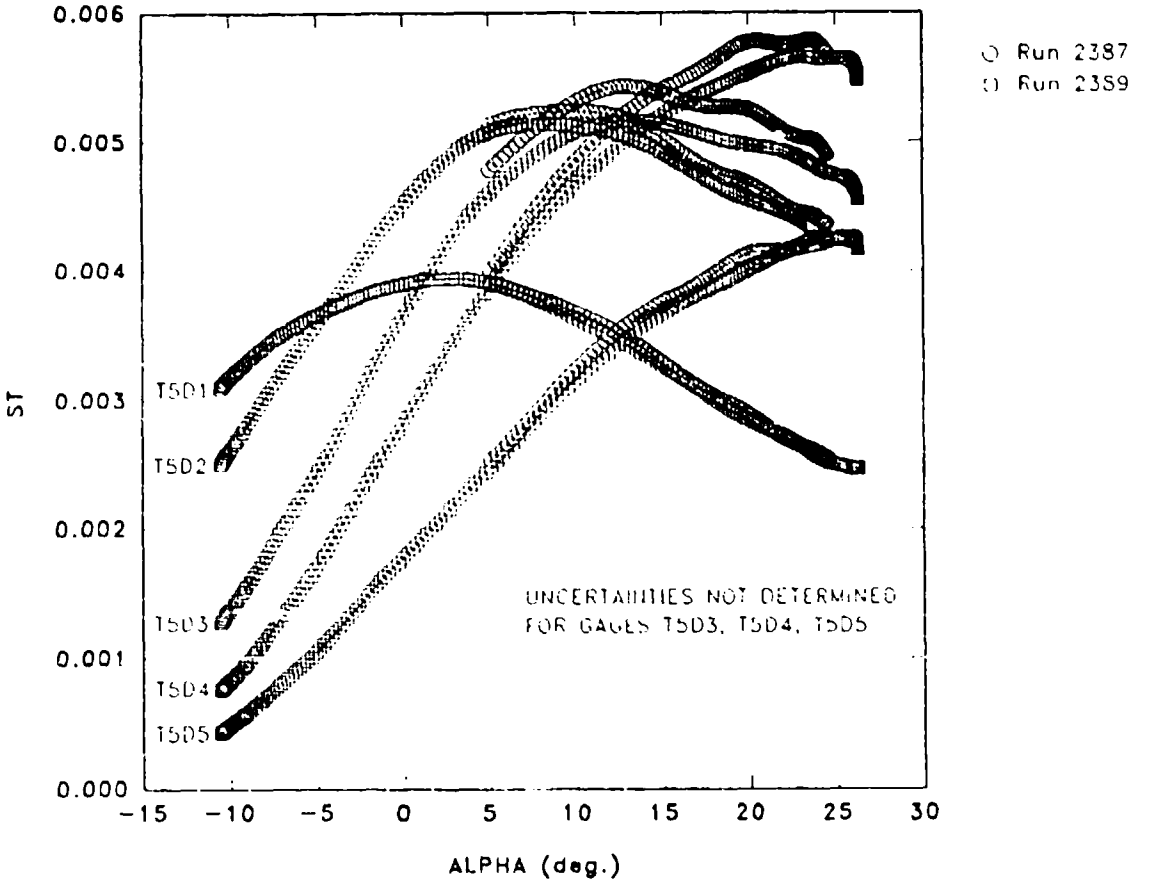

FIGURE 37. MACH-NUMBER EFFECTS ON LEADING-EDGE ST VS. ALPHA

TABLE 1. NOMINAL TEST CONDITIONS

MACH	9.7	10.4	13.9	16.7
P0 (psia)	1,300	14,000	9,400	21,000
T0 (°R)	1,835	1,850	3,050	2,880
REINF (1/ft)	2.0×10^6	20.0×10^6	2.0×10^6	3.2×10^6
QINF (psia)	2.4	23.0	3.2	3.4
UINF (ft/s)	4,650	4,900	6,450	6,400
PINF (psia)	0.037	0.320	0.024	0.018
TINF (°R)	92	90	88	60
Run time (s)	1.5	0.2	1.0	3.0

TABLE 7. ESTIMATED UNCERTAINTIES - CALCULATED PARAMETERS (CONTINUED)

Parameter units	Nominal value	B	P	U_{R}	Comment
P/PT	4.66e-01	3.59e-03	1.58e-03	3.93e-03	REINF = 2.3e+06 ft^{-1}
	8.52e-02	3.95e-04	8.06e-05	4.03e-04	REINF = 20e+06 ft^{-1}
ST*	1.00e-03	-	6% value	6% value	Laminar data
	5.00e-03	-	$-.0912\ ST_t^2$ $+.0107\ ST_t$ +7.88e-5	$-.0912\ ST_t^2$ $+.0107\ ST_t$ +7.88e-5	Transitional/turbulent data. ST_t=d(ST)/d(time)
* ST uncertainties not valid for gages TN, T2D2, T2D3, T5D3, T5D4, T5D5					
AFC	1.21e-01	6.13e-04	6.70e-04	9.08e-04	REINF = 2.3e+06 ft^{-1}
	2.27e-02	7.46e-05	6.23e-05	9.72e-05	REINF = 20e+06 ft^{-1}
ALPHA deg	9.91e+00	8.92e-02	2.90e-02	9.37e-02	All runs
BETA deg	-1.04e+00	4.16e-02	2.38e-02	4.79e-02	All runs
BETAP deg	-1.05e+00	4.20e-02	2.42e-02	4.85e-02	All runs
CAFC	1.20e-01	6.53e-04	6.73e-04	9.37e-04	REINF = 2.3e+06 ft^{-1}
	2.07e-02	8.01e-05	6.27e-05	1.02e-04	REINF = 20e+06 ft^{-1}
CDS	4.02e-01	2.65e-03	1.11e-03	2.87e-03	REINF = 2.3e+06 ft^{-1}
	2.52e-02	1.11e-04	5.56e-05	1.25e-04	REINF = 20e+06 ft^{-1}
CLS	6.49e-02	7.09e-03	3.03e-04	7.09e-03	REINF = 2.3e+06 ft^{-1}
	9.73e-02	6.99e-04	4.47e-05	7.00e-04	REINF = 20e+06 ft^{-1}
CPB	-1.12e-02	1.64e-03	3.30e-04	1.68e-03	REINF = 2.3e+06 ft^{-1}
	-1.14e-02	1.65e-04	3.25e-05	1.69e-04	REINF = 20e+06 ft^{-1}

TABLE 7. ESTIMATED UNCERTAINTIES - CALCULATED PARAMETERS (CONTINUED)

Parameter units	Nominal value	B	P	U_{rss}	Comment
NFC	6.49e-02	7.09e-03	3.03e-04	7.09e-03	REINF = 2,3e+06 ft^{-1}
	9.80e-02	6.99e-04	4.53e-05	7.01e-04	REINF = 20e+06 ft^{-1}
PMC	-4.32e-02	4.60e-03	4.61e-04	4.62e-03	REINF = 2,3e+06 ft^{-1}
	-6.36e-02	4.54e-04	4.05e-05	4.56e-04	REINF = 20e+06 ft^{-1}
PMCS	-4.32e-02	4.60e-03	4.61e-04	4.62e-03	REINF = 2,3e+06 ft^{-1}
	-6.36e-02	4.54e-04	4.05e-05	4.56e-04	REINF = 20e+06 ft^{-1}
RMC	7.89e-04	1.36e-04	2.51e-05	1.38e-04	REINF = 2,3e+06 ft^{-1}
	-7.96e-05	1.80e-05	4.41e-06	1.85e-05	REINF = 20e+06 ft^{-1}
RMCS	8.92e-04	6.10e-04	1.45e-04	6.27e-04	REINF = 2,3e+06 ft^{-1}
	-1.10e-04	2.06e-05	5.82e-06	2.14e-05	REINF = 20e+06 ft^{-1}
YFC	2.19e-03	2.24e-03	4.33e-04	2.28e-03	REINF = 2,3e+06 ft^{-1}
	1.93e-03	2.26e-04	8.06e-05	2.40e-04	REINF = 20e+06 ft^{-1}
YFCS	2.19e-03	2.24e-03	4.33e-04	2.28e-03	REINF = 2,3e+06 ft^{-1}
	1.93e-03	2.26e-04	8.06e-05	2.40e-04	REINF = 20e+06 ft^{-1}
YMC	-1.37e-03	1.52e-03	2.92e-04	1.54e-03	REINF = 2,3e+06 ft^{-1}
	-1.16e-03	1.52e-04	5.35e-05	1.61e-04	REINF = 20e+06 ft^{-1}
YMCS	-1.37e-03	1.52e-03	2.92e-04	1.55e-03	REINF = 2,3e+06 ft^{-1}
	-1.16e-03	1.52e-04	5.34e-05	1.61e-04	REINF = 20e+06 ft^{-1}
XCPP	-6.53e-01	5.40e-04	2.32e-03	2.38e-03	All runs
XCPY	-6.26e-01	8.88e-02	1.20e-02	8.96e-02	All runs